SERI/PR-8136-1-T5
(DE81029633)

DEVELOPMENT OF HIGH EFFICIENCY CASCADE SOLAR CELLS

Annual Report for the Period July 1980—June 1981

By
M. L. Timmons
S. M. Bedair
J. A. Hutchby
J. R. Hauser
M. Simons

July 1981

Work Performed Under Contract No. AC02-77CH00178

Research Triangle Institute
Research Triangle Park, North Carolina

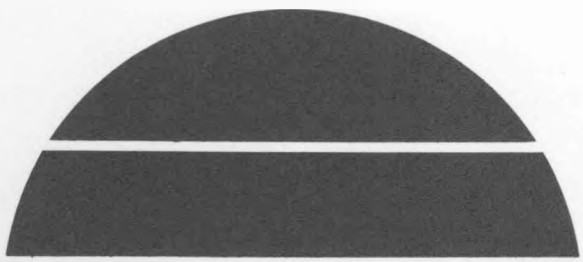

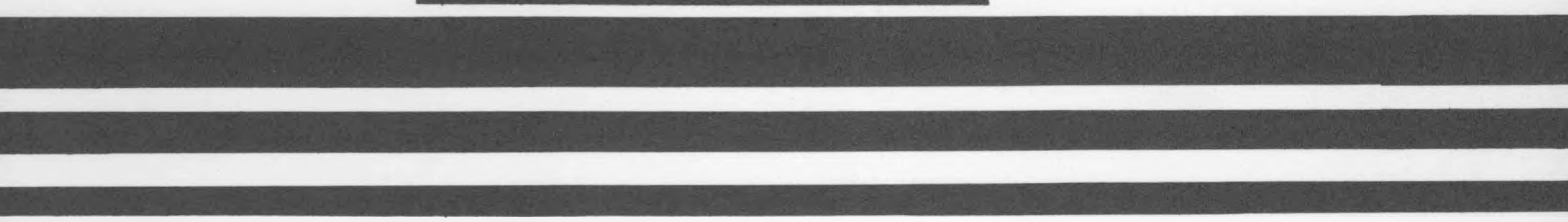

U.S. Department of Energy

Solar Energy

SERI/PR-8136-1-T5
(DE81029633)
Distribution Category UC-63

DEVELOPMENT OF HIGH EFFICIENCY CASCADE SOLAR CELLS

M.L. Timmons, S.M. Bedair, J.A. Hutchby,
J.R. Hauser, and M. Simons

ANNUAL REPORT
for the period
July 1980 to June 1981

Prepared for
Solar Energy Research Institute
Subcontract No. XM-9-81361
Under Contract EG-77-C-01-4042

July 1981

Research Triangle Institute
Research Triangle Park, North Carolina

PREFACE

The work described in this report was conducted in the Semiconductor Research Department of the Research Triangle Institute and in the Department of Electrical Engineering, North Carolina State University, under subcontract to RTI. The work was performed for the Solar Energy Research Institute under contract No. XM-9-8136-1 between July 1, 1980 and June 30, 1981. The SERI technical monitor was K. Mitchell.

Principal authors of this report were M. L. Timmons, S. M. Bedair, J. A. Hutchby, J. R. Hauser (NCSU), and M. Simons. Others playing major roles in the experimental work included T. S. Colpitts, A. D. Brooks, R. A. Connor, G. Kelner, and F. M. Stevens.

TABLE OF CONTENTS

LIST OF FIGURES

ABSTRACT

The principal objective of research conducted under this contract during the past twelve months has been the development and fabrication of two junction cascade solar cells in two different III-V semiconductor materials systems: AlGaAs/GaAs and AlGaAsSb/GaAsSb. Liquid phase epitaxy (LPE) has been successfully used to fabricate experimental cascade cells in both of these materials systems. Additional research has been carried out using organometallic/chemical vapor deposition (OM/CVD) growth technology.

1.0 INTRODUCTION

The monolithic cascade solar cell is one of the most promising devices for significantly increasing photovoltaic power conversion efficiency. The principal objective of research conducted under this contract during the past twelve months has been the development and fabrication of two junction cascade solar cells in two different III-V semiconductor materials systems: AlGaAs/GaAs and AlGaAsSb/GaAsSb. Liquid phase epitaxy (LPE) has been successfully used to fabricate experimental cascade cells in both of these materials systems. Additional research has been carried out using organometallic/chemical vapor deposition (OM/CVD) growth technology.

General material and device requirements as well as theoretical considerations necessary to the fabrication of an optimized two junction, monolithic cascade solar cell have been previously discussed in considerable detail [1-5]. Basically, for optimum high temperature (475 K) performance, the required bottom and top cell bandgaps are approximately 1.2 and 1.8 eV, respectively. Calculations have shown that such a cell should be capable of achieving an AM1, 1 sun efficiency (active area) of about 33% at 300 K and 20.5% at 475 K [3]. At 1000 suns (AM1.5), efficiency values calculated for a two junction 0.95 eV/1.6 eV (not optimized for high temperature operation) cascade cell were approximately 42% at 300 K and 26% at 475 K [2]; thus a 1.2/1.8 eV is expected to be characterized by an active area efficiency somewhat greater than 26% at 475 K and 1000 suns.

Several different III-V materials systems offer optimum bandgap combinations for a two junction cascade cell and have been studied at RTI under previous Sandia and SERI contracts [4-6]. One of the more

promising systems is AlGaAsSb/GaAsSb, which enables fabrication of the entire cascade structure consisting of bottom cell, connecting tunnel junction, top cell, and window layer at the same lattice constant. One disadvantage of this system (and other optimum bandgap systems) is a ≈ 1% lattice mismatch with the GaAs substrate. The AlGaAs/GaAs system, on the other hand, avoids problems stemming from lattice mismatch with the substrate and utilizes a more proven materials technology; although not capable of realizing the 1.8/1.2 eV optimum bandgaps, a 1.9/1.43 eV AlGaAs/GaAs cell should be capable of achieving an AM1, 1 sun efficiency (active area) of approximately 25%. The best experimental cascade cells fabricated at RTI to date have been AlGaAs/GaAs devices with 15 to 16 percent efficiencies (without antireflection coatings); this work is reviewed in Section 2.0. Progress has also been made during the past twelve months in developing AlGaAsSb/GaAsSb cascade cell technology as discussed in Section 3.0. Finally, Section 4.0 reviews OM/CVD research being conducted under subcontract at N. C. State University. The OM/CVD growth technique is being studied as a potential alternative to LPE for cascade cell fabrication.

2.0 GaAlAs/GaAs CELL RESEARCH

2.1 Introduction

Although other III-V materials combinations may offer higher potential cascade cell efficiencies, the AlGaAs ternary system offers a proven material technology that is closely lattice matched throughout its entire compositional range. Consequently, a complete two-junction cascade structure can be grown nearly lattice matched to a GaAs substrate. This advantage is particularly important to obtaining the maximum open-circuit voltage. The energy bandgap range possible for the AlGaAs-GaAs cascade cell, while not providing the optimum value of 0.95 eV for the bottom cell, should still yield an AM1, 1 sun efficiency of 25% for the combination of 1.43 eV for the bottom cell and 1.90 eV for the top cell and tunnel junction.

Fabrication and performance characteristics of the AlGaAs/GaAs cell grown by LPE were described previously [4-7]. Early structures, such as that shown in Figure 2.1a, contained epitaxially-grown, abrupt p-n photovoltaic junctions using the nondiffusing impurities of Sn for n-type material and Ge for p-type layers. Some structures used unintentially doped n-layers ($2 \times 10^{16} cm^{-3}$) for the photovoltaic junction. The better performance characteristics obtained for these structures demonstrated good values of V_{oc} up to 2.2 V, but only modest values of J_{sc} of approximately 5 mA/cm^2. Also, individual $Al_{0.35}Ga_{0.65}As$ top cells were grown using Be diffusion of the photovoltaic junction during the $Al_{0.9}Ga_{0.1}As$ window growth; these exhibited V_{oc} = 1.25 V and J_{sc} = 7 mA/cm^2 without AR

---

* This work was supported mainly by the Air Force Aeropropulsion Laboratory (Contract F33615-78-C-2077).

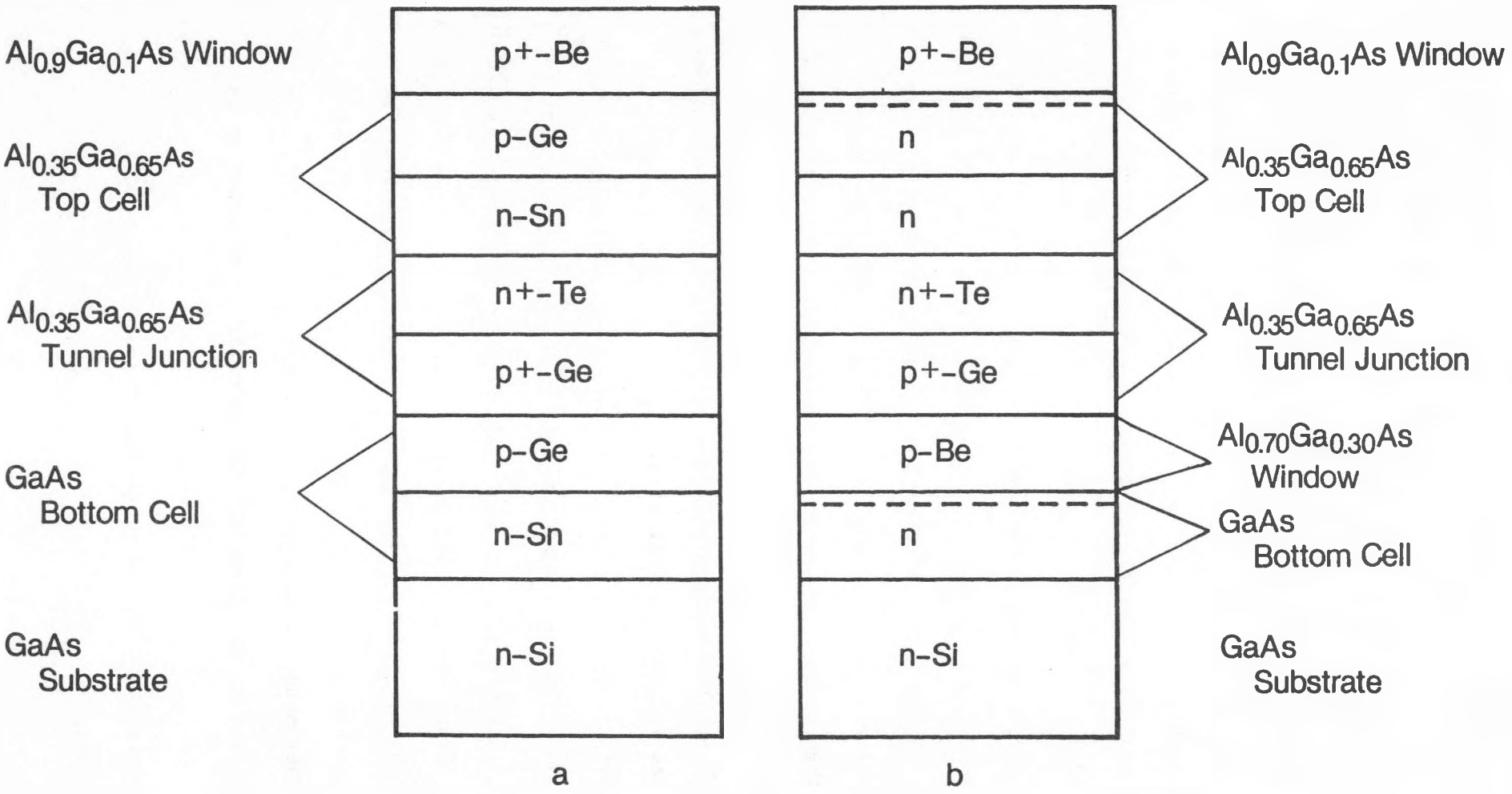

Figure 2.1 AlGaAs Cascade Solar Cell Configuration. a) Original Structure Using Ge and Sn Doped Grown p-n Junction, and b) Current Structure Using p-n Junction Formed by Be Diffused Into Unintentionally Doped n Layers

coating (active area). However, growth of these Be-diffused top cells as part of the cascade structure usually resulted in a deterioration of the open-circuit voltage of the top cell; this was probably due to the propagation of lattice defects from the degenerately doped n+ - p+ tunnel junction.

During the past year, a modified device structure that resulted in a J_{sc} of 13.0 mA/cm^2 (active area without an AR coating) while preserving the V_{oc} of 2.13 V was developed. Combined with a fill factor of 0.74, these results yield a maximum AM0, 1 sun efficiency of 15.1% (≃ 16.4% @ AM1) for cascade structures.

2.2 Modified Structure--Growth and Fabrication

The improved cell structure shown in Figure 2.1b is a seven-layer device epitaxially grown on a GaAs substrate. Compared with the original structure shown in Figure 2.1a, the modified configuration has several key features. These include the following:

1) Both photovoltiac junctions are Be diffused, formed during growth of the $Al_{0.9}Ga_{0.1}As$ layer for the top cell and the $Al_{0.7}Ga_{0.3}As$ layer for the bottom cell. The purpose of this bottom cell window layer is discussed below. Beryllium was used as the p+ dopant for the window layers of both junctions because of its low vapor pressure, necessary for the multiwell LPE growth technique. Doping characteristics and electrical properties of Be-doped AlGaAs have been reported elsewhere [8].

2) As mentioned above, the GaAs diffused junction is achieved by Be diffusion from an $Al_{0.7}Ga_{0.3}As$ window layer. The purpose of this window layer is to reduce the hole concentration in the diffused GaAs junction by using as a diffusion source material $Al_{0.7}Ga_{0.3}As$ which contains a

reduced concentration of Be. It is very difficult to obtain a hole concentration less than mid $10^{18}cm^{-3}$ for Be doped $Al_xGa_{1-x}As$ with $x \leq 0.37$. However, for $x > 0.5$ hole concentrations in the high $10^{17}cm^{-3}$ to low $10^{18}cm^{-3}$ can be routinely achieved. This will allow the carrier concentration on the p-side of the GaAs junction to be limited to the high $10^{17}cm^{-3}$ range, thereby maintaining a better electron diffusion length.

3) The active n-$Al_{0.35}Ga_{0.65}As$ layer of the top cell is epitaxially grown on an additional layer of the same composition. This additional layer reduces the propagation of defects originating in the n+ Te - p+ Ge tunnel junction [9]. Also, as described below, the technique for preparing the LPE melts for growing the tunnel junction was changed to reduce defects generated in the Te doped layer. Properties of the tunnel junctions have been reported previously [10]. Currently, a p+ GaAs:Ge cap layer is grown on top of the $Al_{0.9}Ga_{0.1}As$ layer to serve as a p+ contact. As discussed below, the excess p+ GaAs is selectively etch-removed using the finger contact metallization as the etch mask.

In addition to these structural changes, modifications were also made to the LPE technique for growing the devices. Standard features of this process include use of a horizontal, multibin, graphite sliding boat used in a horizontal growth furnace containing a 24" or 36" sodium-filled heat pipe. Silicon doped, <111>A&B oriented GaAs substrates ($n \simeq 10^{18}cm^{-3}$) are polished and etched prior to growth. Growth is initiated at 800°C with a constant cooling rate of 0.6°C/minute.

Modifications to the growth process include:

1) Increasing the cooling rate for the LPE growth to 1°C/minute, thus reducing exposure of the tunnel junction layers to high temperature

during the period of growing the top cell. This maintains the abruptness of the tunnel junction and thereby improves the fill factor.
2) Developing a new procedure for preparation of the tunnel junction melts to reduce defect formation, particularly in the Te doped, n+ layer. Tellurium tends to form compounds both with Ga and with Al such as Al_2Te_3, GaTe, etc. These compounds form precipitates that create and propagate lattice defects in the top $Al_{0.35}Ga_{0.65}As$ cell. Growth at temperatures above 900°C has been found to eliminate the formation of these unwanted compounds. However, this temperature is too high to obtain the necessary abrupt doping profile which the tunnel junction requires. This difficulty was significantly reduced in the present study by performing the growths at 800°C according to the following procedure.

Gallium and GaAs for the n+ Te melt and Ga, Ge, and GaAs for the p+ Ge melt were baked together at 900°C for two hours and then quenched to room temperature. Then Te and Al were added to the n+ melt and Al to the p+ melt. The remainder of the melts and wafers required for the cascade cells were also loaded. The completely loaded boat was then reheated to the starting growth temperature of 800°C, baked for 4 hours, and the growth performed. This procedure provided smooth, specular AlGaAs epitaxial layers free of the previously observed surface irregularities common to the Te doped n+ layer.

An SEM photomicrograph taken in the secondary emission mode together with an electron-beam-induced current (EBIC) trace is shown in Figure 2.2. Also, for comparison more typical values for layer thicknesses and doping concentrations are shown in Table 2-1.

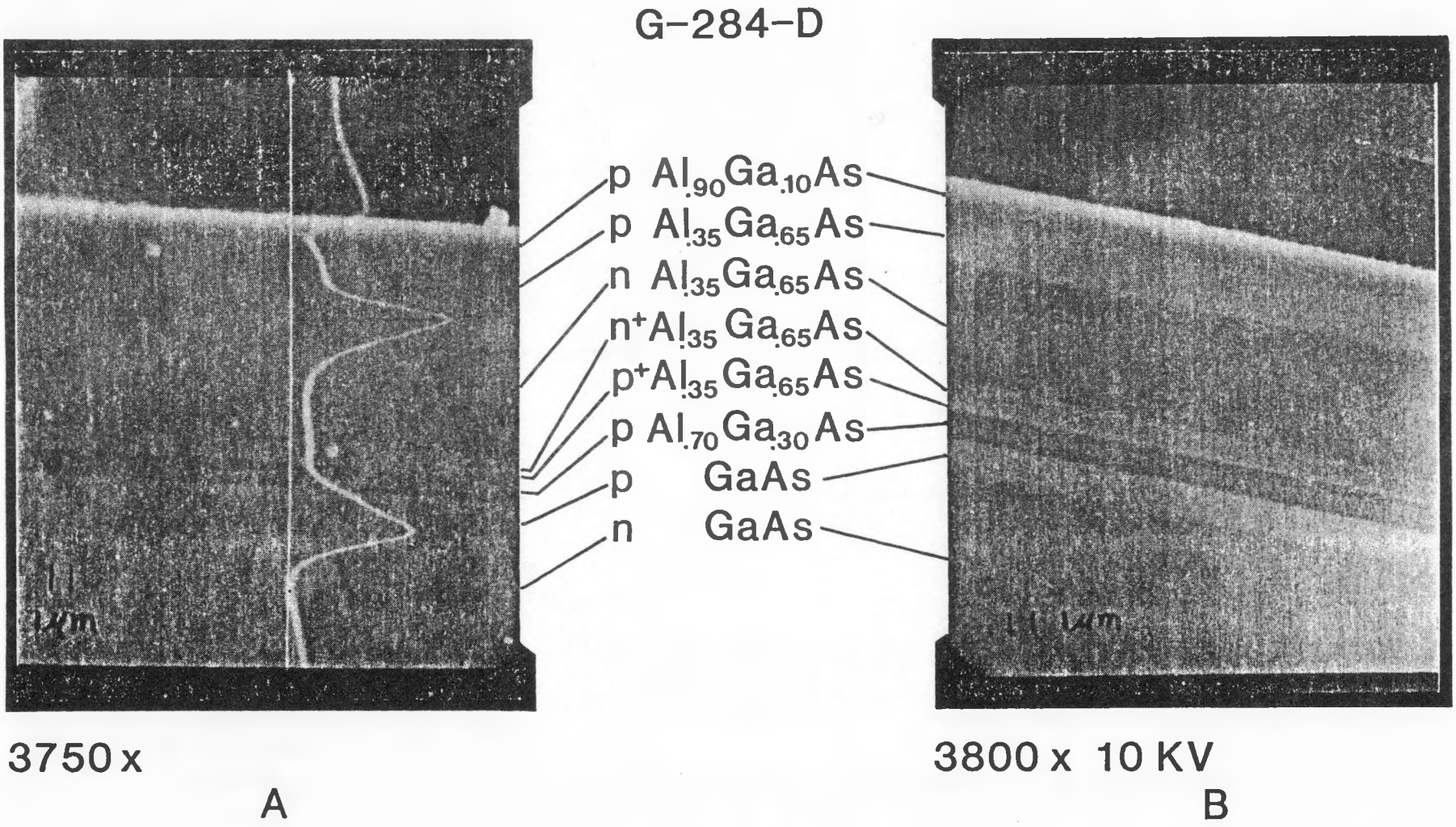

Figure 2.2 Scanning Electron Micrographs of an AlGaAs-GaAs Cascade Solar Cell Cross Section. a) Secondary Emission Mode Only, and b) Combined Secondary-Emission and Electron-Beam-Induced-Current Modes

Layer	n	p	Thickness (μm)	AlAs(%)
p+-AlGaAs (window)		2×10^{18}(Be)	0.2	90
n-AlGaAs	5×10^{16}		4.5	35
n-AlGaAs	5×10^{16}		0.5	35
n+-AlGaAs	5×10^{18}(Te)		0.4	35
p+-AlGaAs		5×10^{18}(Ge)	0.4	35
p+-AlGaAs (window)		1×10^{18}(Be)	0.5	70
n-GaAs	5×10^{16}		4	

Table 2-1 Composition, Impurity Concentrations, and Thickness of Each Layer in a Typical AlGaAs-GaAs Cascade Solar Cell

Fabrication of the 1 cm^2 wafers into photovoltaic devices was completed by use of a photolithographic process to develop openings in a positive resist for sequential evaporation of a five-level metallization for the top contact to the p+ layer. This metallization consists of Mg (200 Å), Ti (300 Å), Pd (300 Å), Ag (1500 Å), and Al (1500 Å). The evaporation is performed in an e-beam system at 10^{-7} torr. Sn (300 Å) and Ag (2000 Å) are then e-beam evaporated to the back surface. Removal of the photoresist from the front surface is followed by sintering of the contacts in flowing H_2 at 550°C for 3-4 minutes. The area of each cell was defined by etching a mesa of $1.2 \times 10^{-2} cm^2$, and the excess p+ Ge doped GaAs contact layer was selectively etched using $NH_4OH:H_2O_2$ (approximately 60:1 by volume) pH adjusted to 7.05 ± .05. Wafers selected for complete evaluation were wire bonded into a flatpack package and a two-layer AR coat e-beam evaporated. The AR coat usually consists of 560 Å Ta_2O_5 followed by 800 Å of SiO_2.

2.3 Device Performance

2.3.1 Cascade Cell Without AR Coating

The modifications to the device structure and growth process have resulted in substantial improvements in the cell performance, particularly in short-circuit current density. The terminal I-V characteristic of a complete cascade cell is shown in Figure 2.3. Improved active-area short-circuit current densities up to 13 mA/cm^2 for AM0 and 12 mA/cm^2 for AM1 have been obtained for devices not having an AR coating. These current densities, increased by 28% to account for an AR coating, are equal to one half of the J_{sc} reported for the best GaAs single-junction solar cell and are near the maximum expected for the two-junction

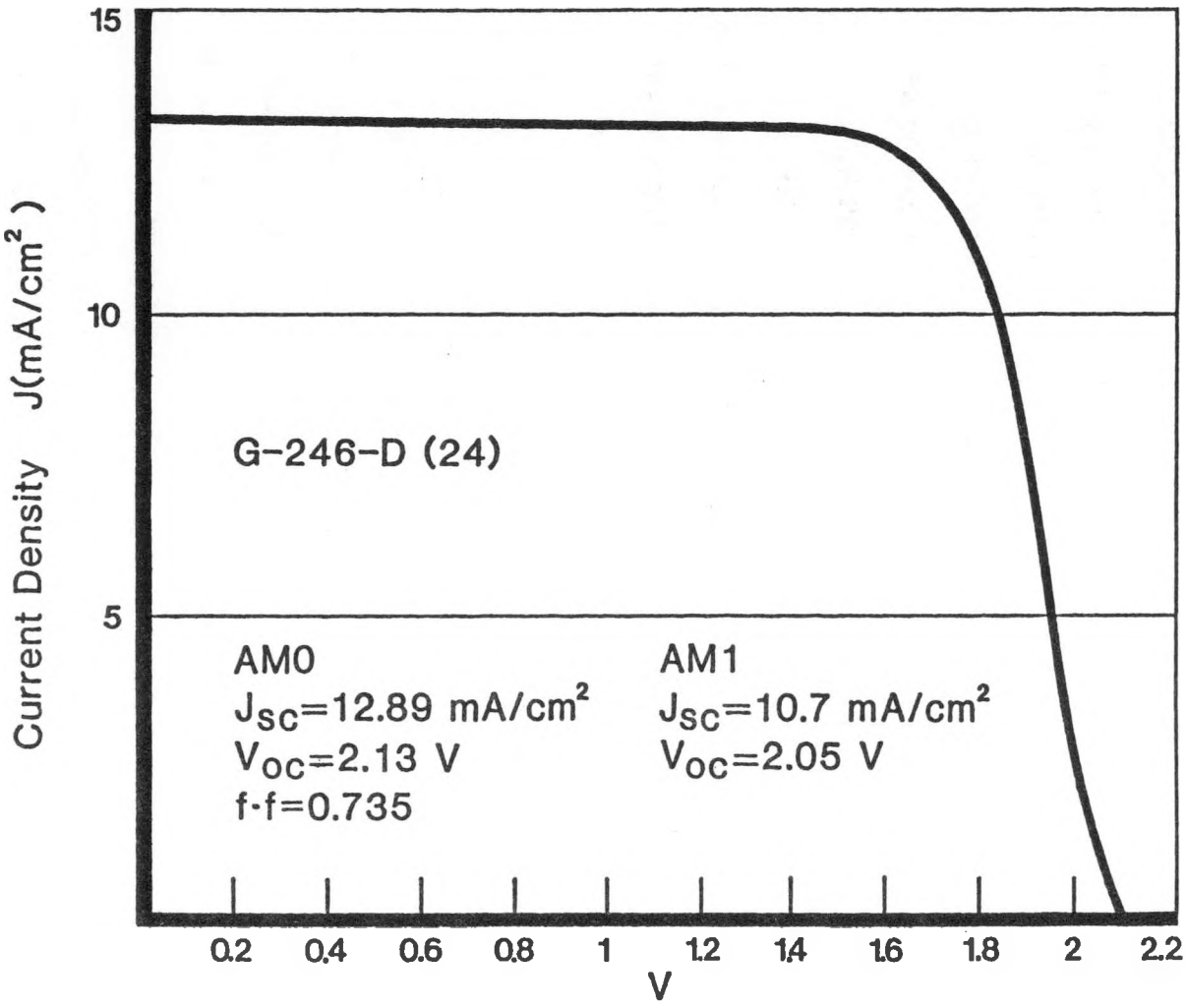

Figure 2.3 Current-Voltage Characteristic for AlGaAs-GaAs Cascade Solar Cell

AlGaAs-GaAs cascade cell. This is because each cell in a current matched cascade device absorbs one half of the solar spectrum absorbed by a single junction GaAs cell and, therefore, produces half the current of a GaAs device. The best cascade cell fabricated to date had an active area power conversion efficiency of 15.1% AM0 and 16.4% AM1.5 without an AR coating.

2.3.2 Cascade Cells With AR Coating

To maximize efficiency of a cascade solar cell the current generated by both the low bandgap and the high bandgap junctions has to be equal (i.e., matched). In a cascade cell for which the currents generated by the two junctions are mismatched, the cascade current will be limited by the cell generating the lower current. The conditions for current matching depend primarily on the bandgap combinations, the spectrum of the solar radiation, and the AR coating.

The effect of an AR coating on cell performance is illustrated in Figures 2.4 and 2.5 which show the spectral response and load curves, respectively, for an AlGaAs-GaAs cascade cell. This particular cell had a top-cell bandgap of 1.9 eV capped by a window layer. The spectral response measurement was made using a chopped light source in conjunction with a filter wheel containing 15 filters covering the spectral range from 0.40 μm to 1.10 μm in 0.05 μm increments. The short wavelength response, corresponding to the top cell, was obtained with a d.c. light source filtered to transmit $\lambda > 0.72$ μm to turn on the bottom cell. The longer wavelength response, corresponding to the bottom cell, was obtained using a filtered d.c. light source transmitting in the range 0.38-0.60 μm (10% transmission points) to turn on the top cell.

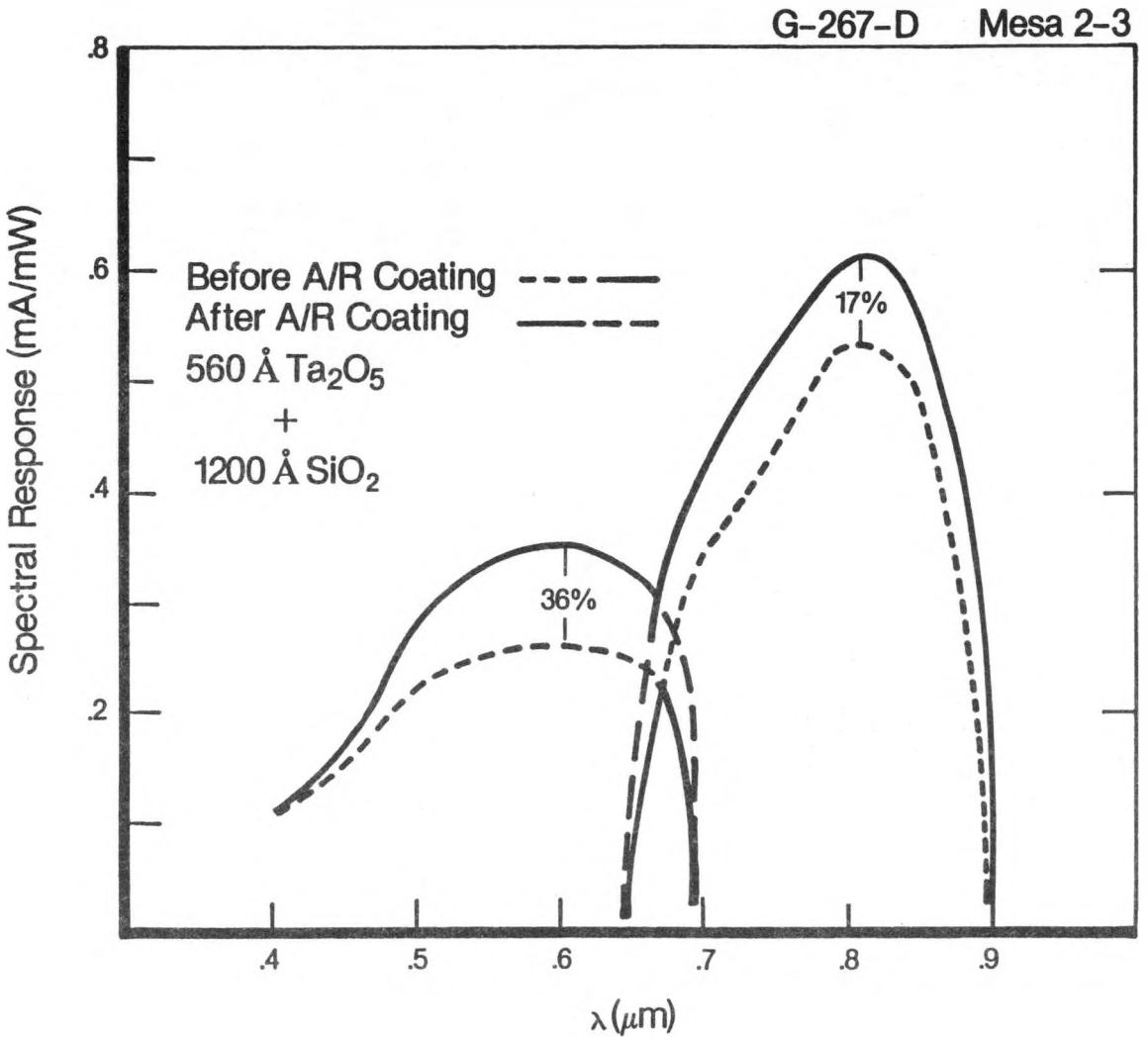

Figure 2.4 Spectral Response for AlGaAs-GaAs Cascade Solar Cell Sample G-267-D

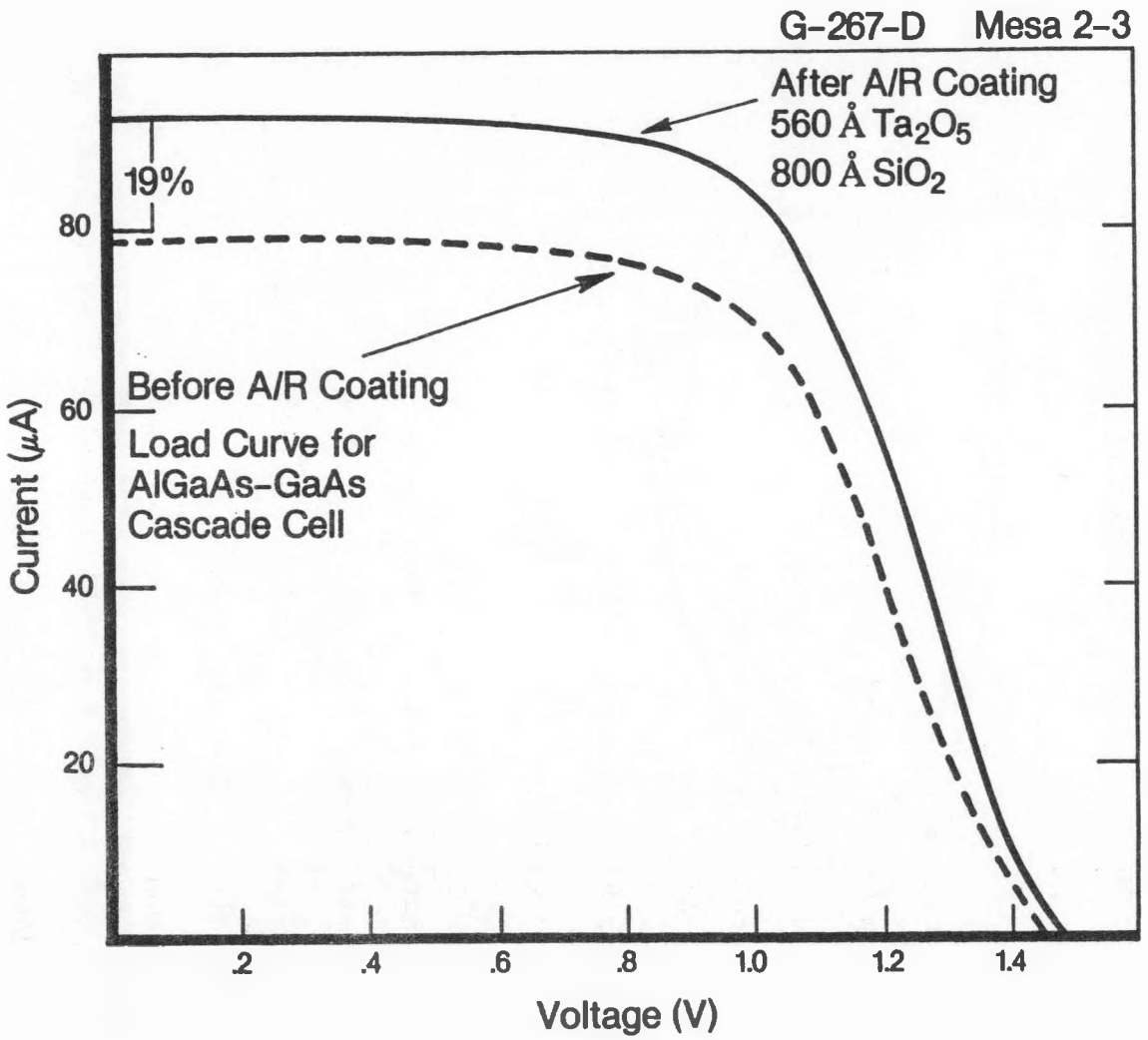

Figure 2.5 Illuminated Current-Voltage Characteristics for an AlGaAs-GaAs Cascade Solar Cell, Sample G-267-D

The load curve measurement was made using an electronic load together with a xenon lamp filtered with 2" water and calibrated using a blue-sensitive, calibrated Si solar cell obtained from NASA-Lewis Research Center. Application of the AR coating (560 Å Ta_2O_5 + 1200 Å SiO_2) to this cell increased the spectral response of the top cell a larger percentage than that of the bottom cell. Therefore, a cascade cell which was current matched prior to application of the AR coat would be limited by the bottom cell afterwards.

Comparison of the fractional increase in I_{sc} given in the load curve of Figure 2.5 with the increases for the peak spectral responses of the top and bottom cells given in Figure 2.4 illustrates another characteristic of cascade cells. That is, for a current-mismatched structure, the maximum increase of I_{sc} which can be obtained from a cascade cell following deposition of an AR coat is determined by the limiting cell. In the case of this example, the bottom cell limits the cascade current.

Figures 2.6 and 2.7 show another example of an AlGaAs-GaAs cascade cell for which the AR coat increased the peak spectral response (Fig. 2.6) of top and bottom cells by 27 and 28%, respectively; this is reflected in a 28% increase in the cascade short-circuit current (Fig. 2.7). These results illustrate 1) that the AR coat can affect the current-match condition, and 2) that a two-layer AR coat can increase the current of a properly matched cascade cell by 28% or more.

2.4 Effect of High Solar Concentration and High Temperature

At high solar concentrations, approaching 50 suns, the tunnel junction starts to show some undesirable effects depending on its

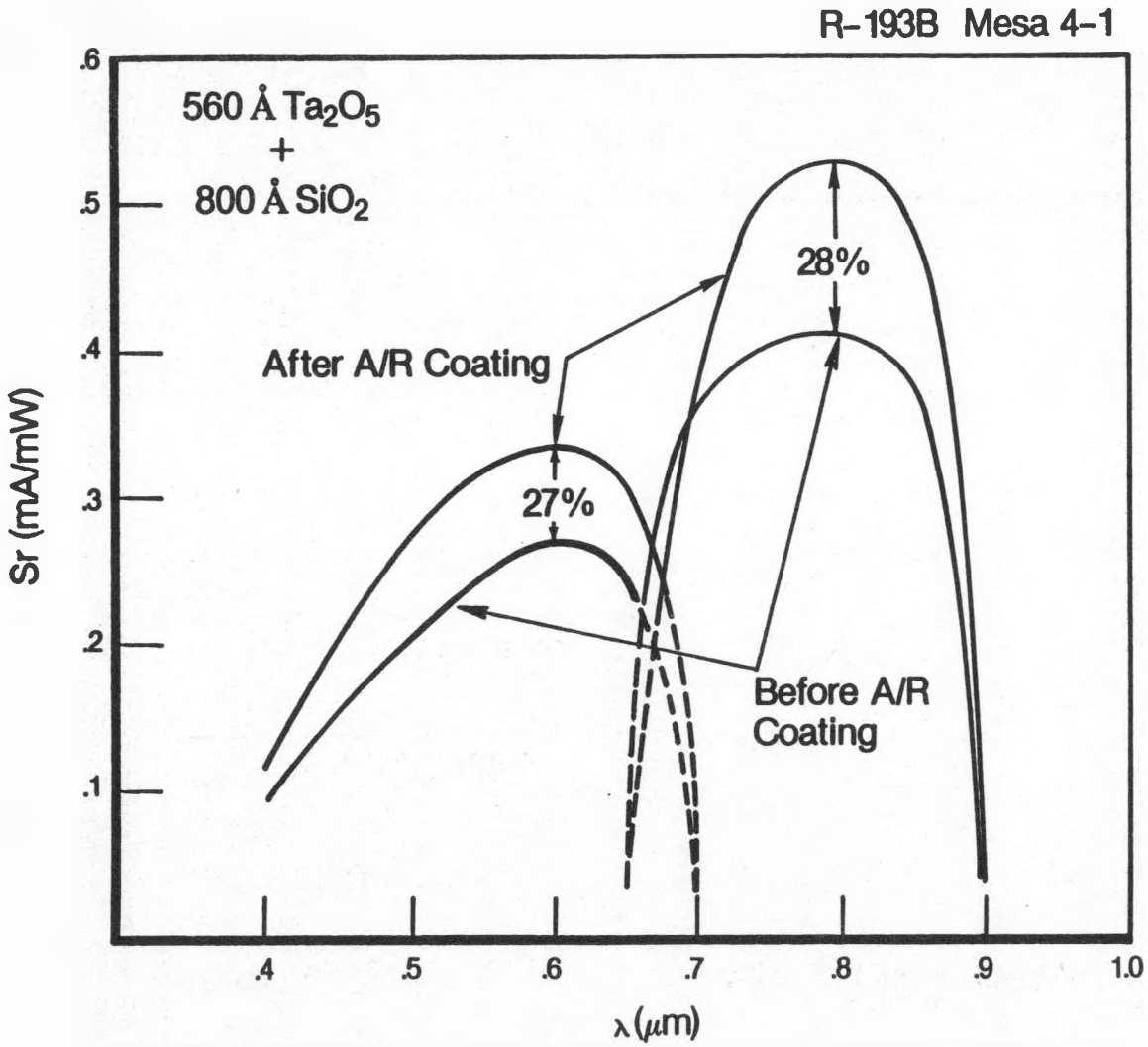

Figure 2.6 Spectral Response of AlGaAs-GaAs Cascade Solar Cell, Sample R-193B

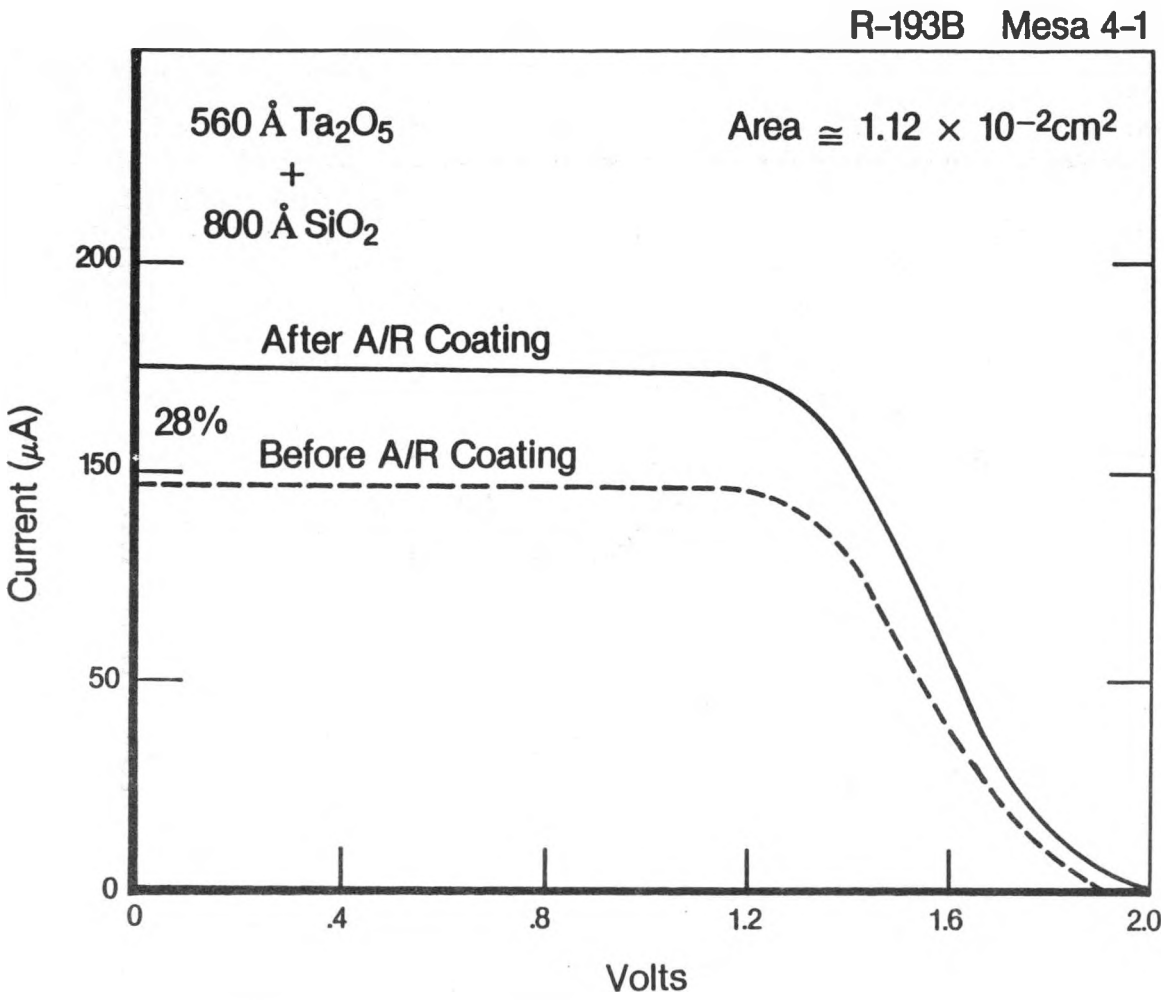

Figure 2.7 Illuminated Current-Voltage Characteristics for an AlGaAs-GaAs Cascade Solar Cell, Sample R-193B

abruptness and bandgap energy. High series resistance (and in some cases a negative resistance region) are observed in the I-V characteristics as shown in Figures 2.8a and 2.8b, respectively. At high temperature and high concentration, the negative resistance or the nonlinear portion of the I-V characteristics completely disappeared, as shown in Figures 2.9a and 2.9b, due to the exponential temperature dependence of the excess current. The effect of temperature on the V_{oc}, I_{sc} and efficiency of a cascade cell at 1 sun, AM0 is shown in Figure 2.10.

2.5 Summary

AlGaAs-GaAs monolithic cascade solar cells with active-area efficiencies up to 15.1% AM0 and 16.4% AM1 without AR coatings have been fabricated. The largest short-circuit current densities obtained from these structures have nearly reached the maximum expected. However, additional improvements in the open-circuit voltage and fill factor are needed to reach the maximum AM1 efficiency goal of $\geq$ 25% predicted for these devices. The condition for matching the photocurrent generated by the two component junctions has been demonstrated by a continuing process of optimizing the cell parameters. A two-layer antireflection coat of Ta_2O_5 and SiO_2 has been shown to increase the short-circuit current of a properly current-matched cascade cell by 28%. Effects of high temperature and high solar concentration on the cell performance have been examined.

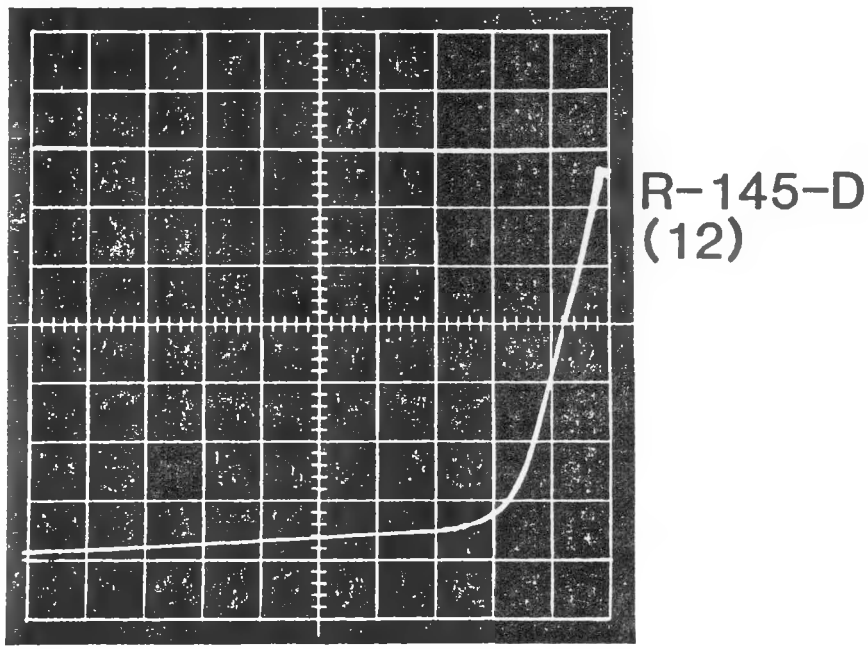

A

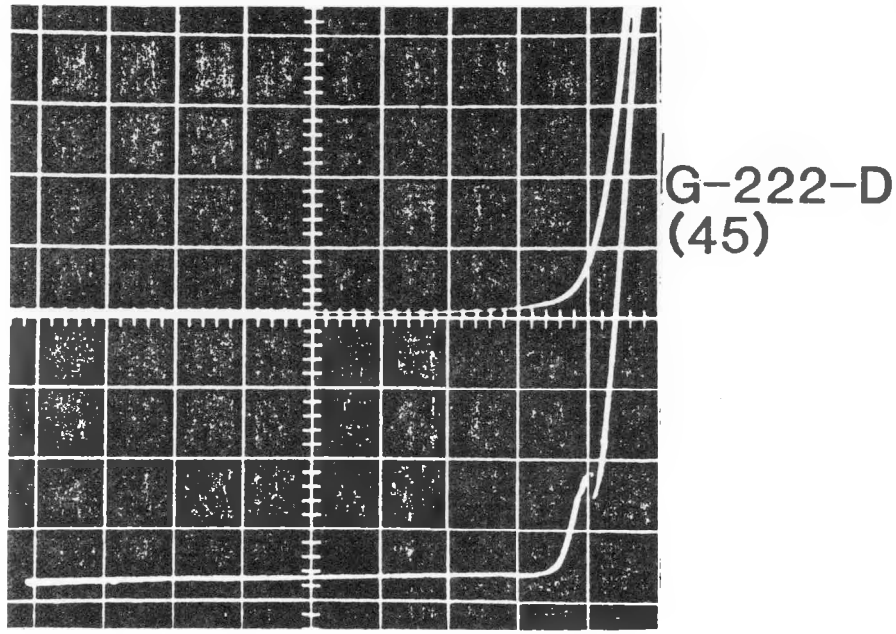

B

Figure 2.8 Dark and Illuminated Current-Voltage Characteristics Showing Various Effects of Tunnel Junction at High Solar Concentration (~50 suns) a) High Series Resistance b) Negative Resistance Characteristic. Vertical Scale: 2 mA/div; Horizontal Scale: 0.50 V/div.

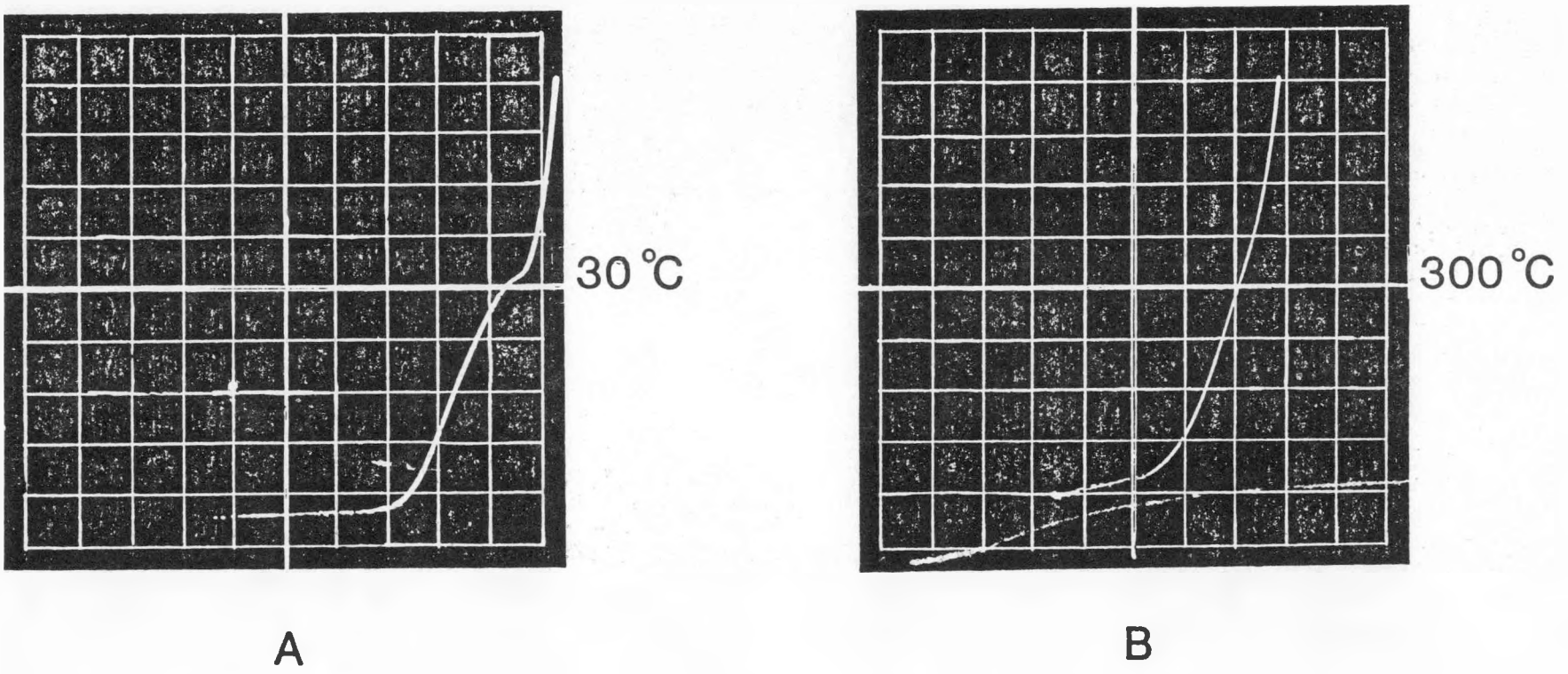

Figure 2.9 Illuminated Current-Voltage Characteristics of an AlGaAs-GaAs Cascade Solar Cell at High Solar Concentration (~50 suns) and High Temperature: a) 30°C; and b) 300°C. Vertical Scale: 2 mA/div; Horizontal Scale: 0.50 V/div.

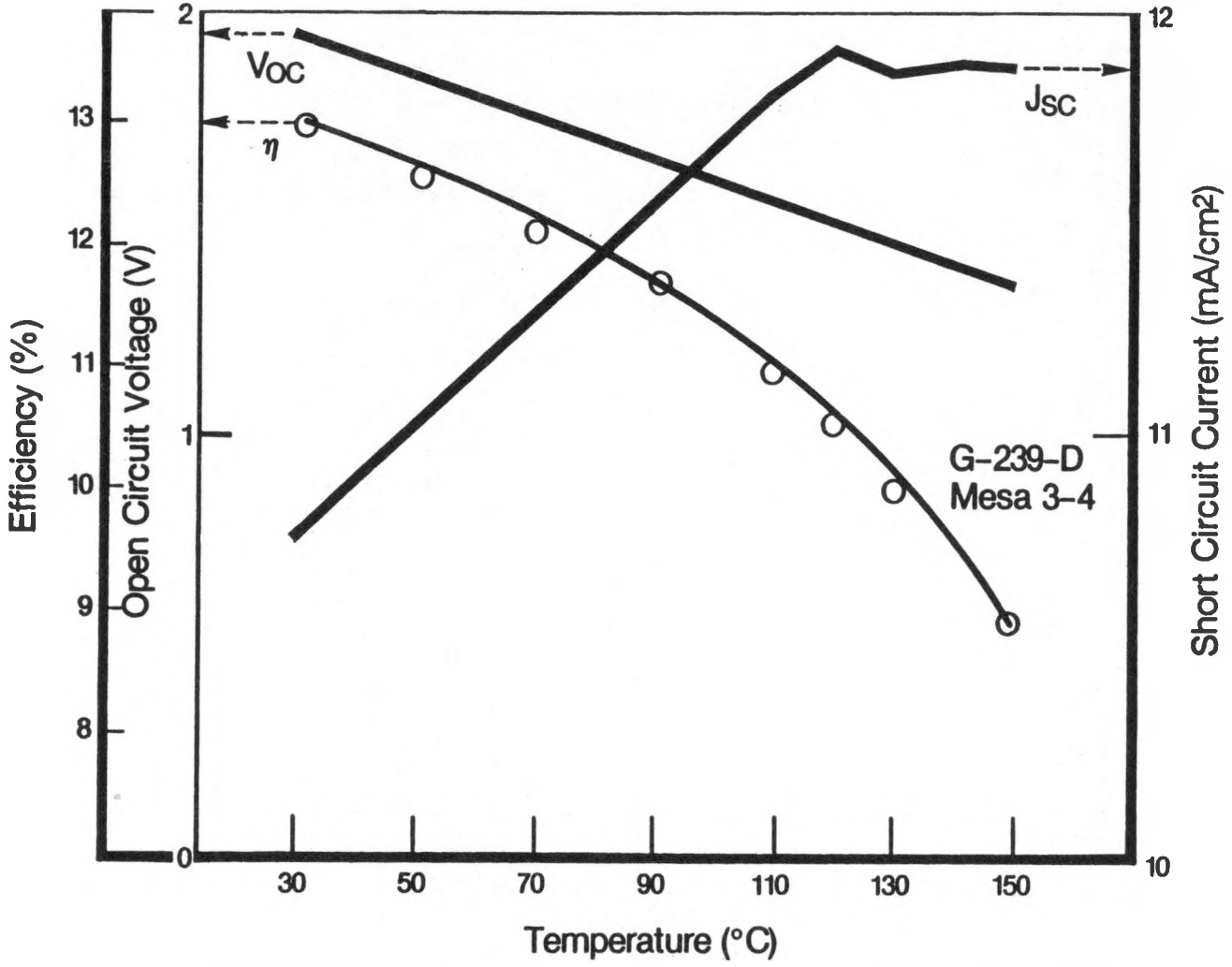

Figure 2.10 Open Circuit Voltage, Short Circuit Current Density, and Power Conversion Efficiency Versus Temperature for an AlGaAs-GaAs Cascade Solar Cell

Blank Page

3.0 AlGaAsSb/GaAsSb CASCADE CELL DEVELOPMENT

Considerable progress in developing the AlGaAsSb/GaAsSb cascade cell materials system has been achieved during the past year. The most significant accomplishments include the following:

1) Development of Mg- and Be-diffused junctions for both the GaAsSb bottom cell and the AlGaAsSb top cell grown separately has resulted in dramatic improvements in the short circuit current density (J_{sc}) of each cell; J_{sc} values greater than 20 mA/cm^2 and 8 mA/cm^2 have been measured for bottom and top cells, respectively.

2) The two-layer antireflection (AR) coating consisting of ≈ 560 Å of Ta_2O_5 and ≈ 800 Å of SiO_2 has been demonstrated to increase J_{sc} typically more than 20% in individual top and bottom cells.

3) New twelve-well graphite boats have permitted the growth of structures with greater numbers of matching layers. Use of these boats has resulted in more consistently good surface morphologies.

These and other developments are discussed in the following paragraphs for the bottom and top cells as well as for the overall cascade structure. Experimental results for both abrupt and diffused junctions are presented.

3.1 GaAsSb Bottom Cell Development

3.1.1 Abrupt Junctions

The initial antimonide work employed Ge as the p-type dopant; since Ge has little tendency to diffuse, abrupt p-n junctions were formed. For junctions with a 1.2 eV bandgap, typical ranges of values for V_{oc}, J_{sc}, and fill factor (FF) were 0.5 to 0.55 V, 3 to 5 mA/cm^2, and 0.6 to 0.7, respectively. The I-V characteristic of the best abrupt junction sample is shown in Figure 3.1; this sample has V_{oc}, J_{sc}, and FF values of 0.55 V, 7 mA/cm^2, and 0.68, respectively.

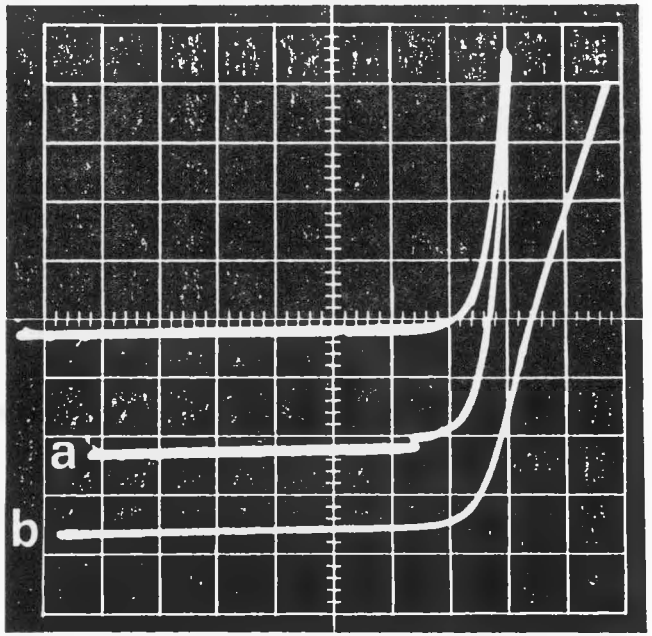

p-$GaAs_{0.88}Sb_{0.12}$	Bottom Cell
n-$GaAs_{0.88}Sb_{0.12}$	
n-$GaAs_{0.88}Sb_{0.12}$	Matching Layers
n-$GaAs_{0.88}Sb_{0.12}$	
n-$GaAs_{0.92}Sb_{0.08}$	
n-$GaAs_{0.96}Sb_{0.04}$	
n-GaAs	Substrate

Bottom Cell at	a) 1 Sun	b) 30 Suns
	0.2V/div	0.2V/div
	0.01mA/div	0.2mA/div
	V_{oc}~0.55	V_{oc}~0.7V
	J_{sc}~7mA/cm^2	J_{sc}~200mA/cm^2

Figure 3.1 GaAsSb Abrupt Junction

Both V_{oc} and J_{sc} for these Ge-doped samples are lower than anticipated. Based on the ideal diode equation and linear extrapolation of the salient material parameters for GaAs and GaSb, V_{oc} values of 0.65 to 0.70 V were expected for GaAsSb diodes with 1.2 eV bandgaps at 1 sun (AM0) illumination. The 0.8% lattice mismatch between the GaAs substrate and the bottom cell is believed to cause the low V_{oc}, and it is this mismatch which necessitates the matching layers shown in Figure 3.1; at least two matching layers were used in all growths of the compositions of interest.

The low J_{sc} value probably resulted from two principal contributions: bulk recombination due to short minority carrier diffusion length and interfacial recombination at the p-n interface in the abrupt junctions. Both of these phenomena would lower the carrier collection efficiency, and, indeed, these diodes characteristically have quantum efficiencies of only a few percent.

The diode factor, n, on all the abrupt jucntions was very near 2, indicating current domination by space charge recombination. The best value measured was 1.8.

Finally, V_{oc} decreased very rapidly with increasing temperature as is shown in Figure 3.2, and at 150°C (curve e in Figure 3.2), it has decreased to $\simeq$ 50% of the room temperature value.

3.1.2 Diffused Junctions

Because of the relatively poor performance of abrupt junctions and the success of diffused junctions in the AlGaAs and GaAs, examination of diffused junctions was undertaken in GaAsSb. Some loss of flexibility in growth sequences was encountered because of considerations for the diffusive nature of the dopants; and this can be considered the most serious drawback of the diffused junction.

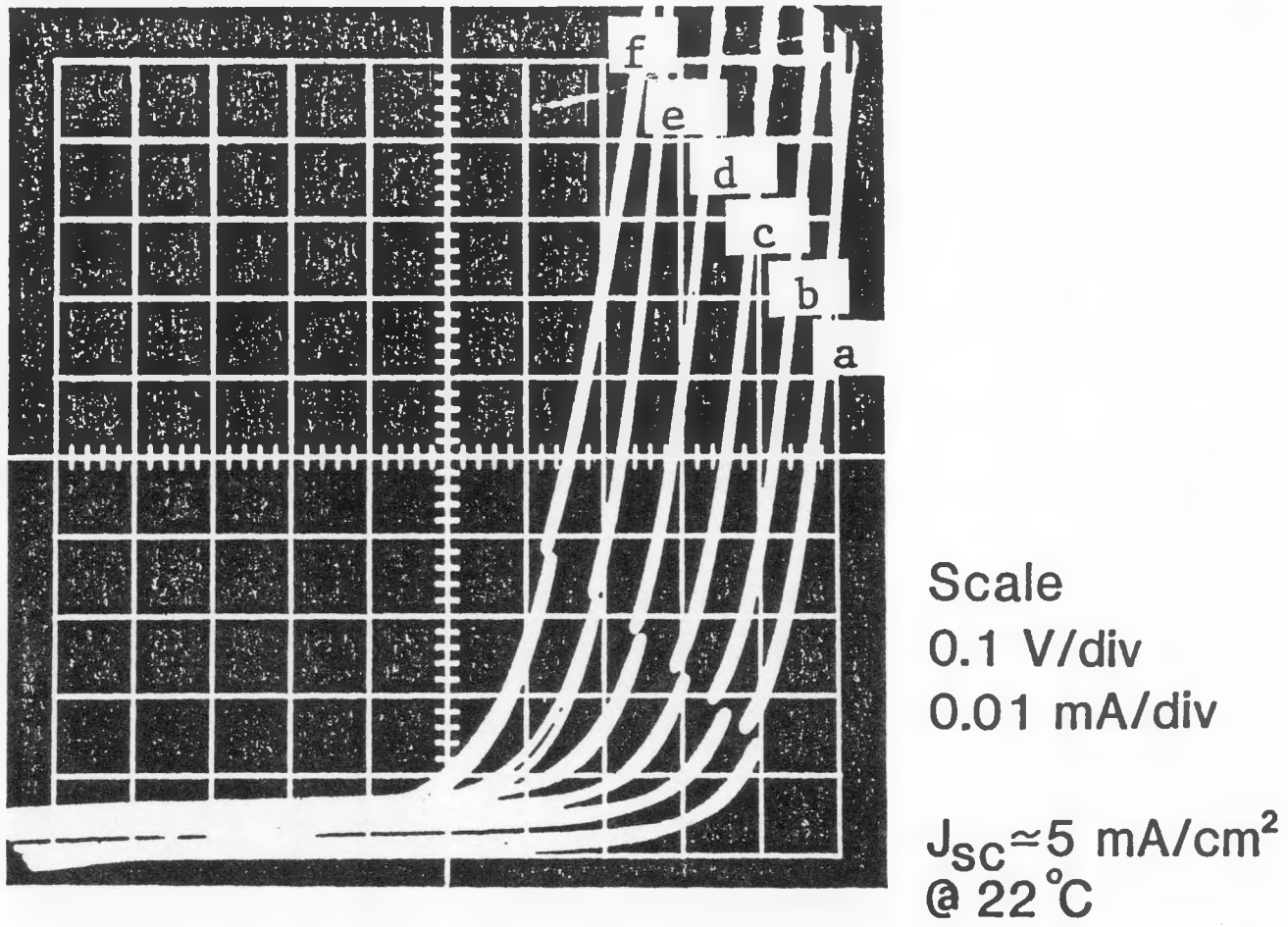

Figure 3.2 I-V Curves for GaAsSb Bottom Cell at
a) 22°C, b) 60°C, c) 90°C, d) 120°C, e) 150°C, and f) 180°C

Four dopants, Cd, Zn, Mg, and Be, were considered for the p-type diffusant. Cd and Zn were discounted because of their high vapor pressure and the accompanying tendency to leave a melt and possibly contaminate other melts and substrates. Beryllium, the most attractive specie based on AlGaAs results, is extremely toxic and requires an enclosed growth system; therefore, initial studies used Mg while a Be growth system was being fabricated.

Figure 3.3 shows the I-V curve of a typical Mg-diffused bottom cell (1.2 eV). V_{oc} is ≃ 0.52 V, still lower than expected, but J_{sc} has increased to ≃ 9.6 mA/cm^2. With a FF of 0.65, the efficiency of this diode (based on active area) was almost 2.5%. The increased J_{sc} is also reflected in the quantum efficiency illustrated in Figure 3.4 which shows a peak value greater than 35% and is generally quite responsive over the entire frequency range anticipated for the bottom cell. The I-V curve of a cell and tunnel junction is shown in Figure 3.5. These characteristics are almost identical with those of Figure 3.3, indicating that the tunnel junction does not affect bottom cell performance. Shown in Figure 3.6 is the I-V curve of the Mg-doped junction which has yielded the highest current density (15 mA/cm^2) to date. Note that the FF and V_{oc} for this sample are practically identical to other samples and are very similar to Ge-doped samples. The temperature dependance of V_{oc} is shown in Figure 3.7 and is approximately 50% of that at room temperature without significant J_{sc} change.

As described above, the improvement in diffused junction performance is mainly related to increasing the carrier collection. The diode factors and V_{oc}'s are within the range of those measured for abrupt junctions. With diode factors near 2.0, current is still being controlled by depletion region recombination.

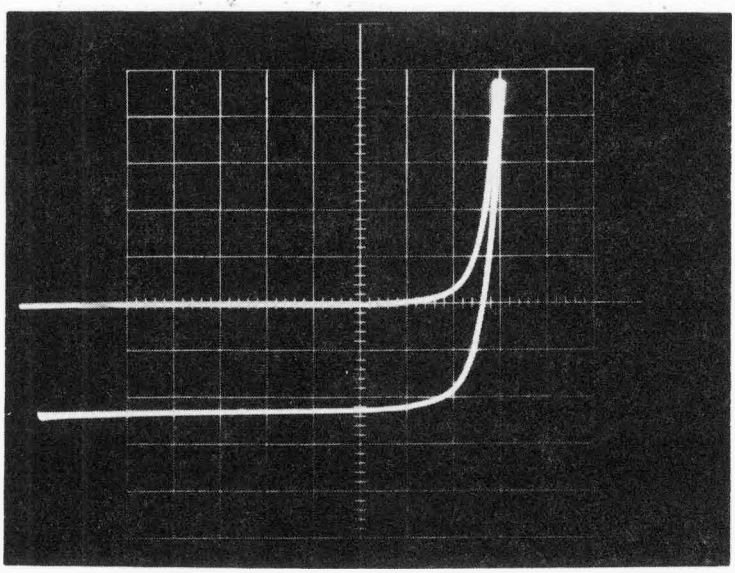

Vert = 0.1 mA/div Hor = 0.2 V/div

($V_{oc} \simeq 0.5$ V, $J_{sc} \simeq 9.6$ mA/cm^2)

Figure 3.3 Mg-Diffused GaAsSb Bottom Cell (1 sun, AM0)

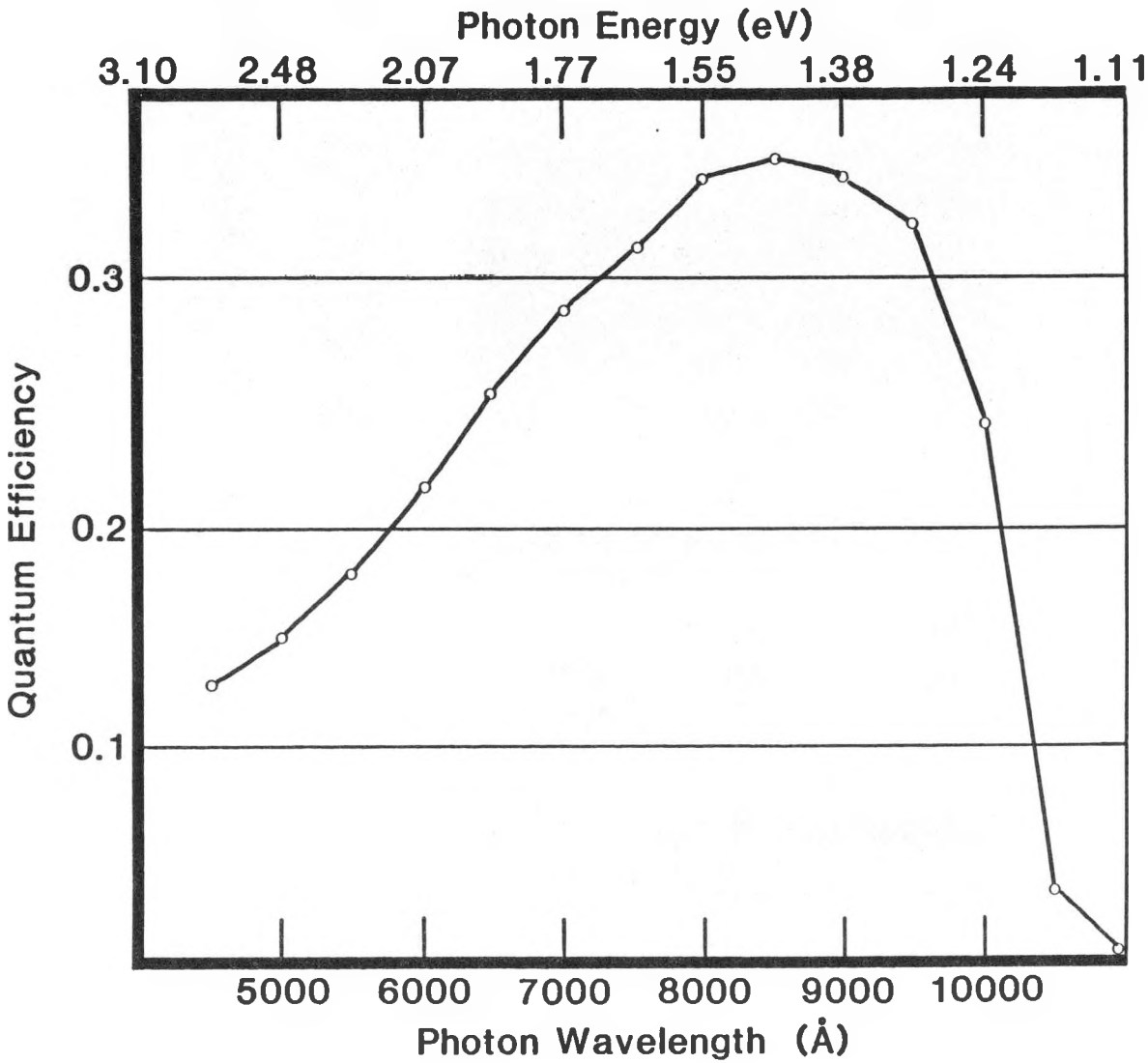

Figure 3.4 Quantum Efficiency of Mg-Diffused GaAsSb Bottom Cell

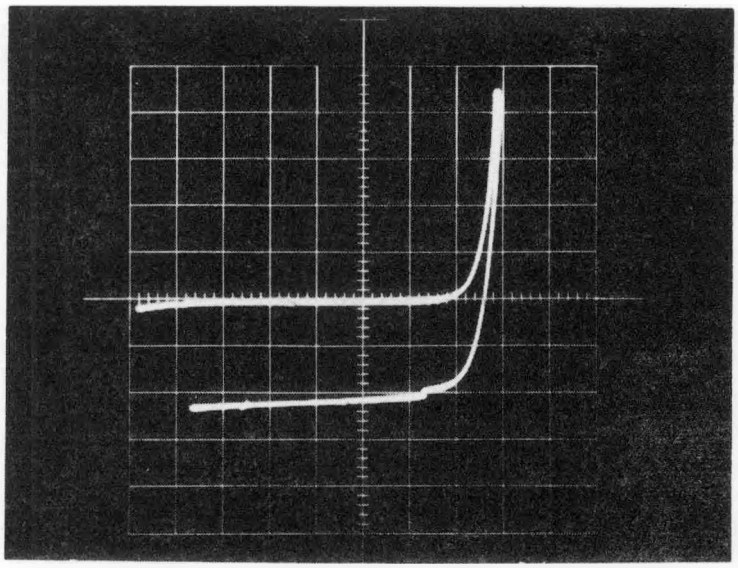

Vert = 0.02 mA/div Hor = 0.2 V/div

($V_{oc} \simeq 0.53$ V, $J_{sc} \simeq 8.6$ mA/cm^2)

Figure 3.5 Mg-Diffused GaAsSb Bottom Cell with AlGaAsSb Tunnel Junction Grown on Top (1 sun, AM0)

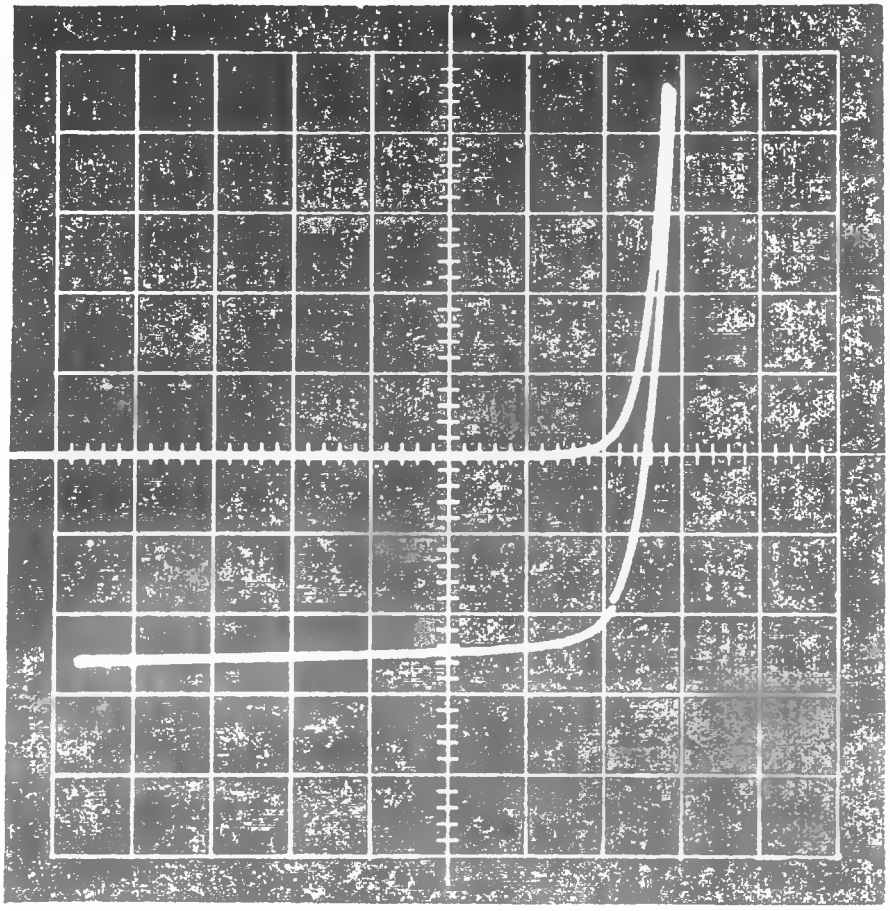

$V_{oc} \simeq 0.52$ V, $J_{sc} \simeq 15$ mA/cm^2, FF $\simeq 0.64$

Figure 3.6 I-V Curve of Best Mg-Diffused GaAsSb Junction (1 sun, AM0)

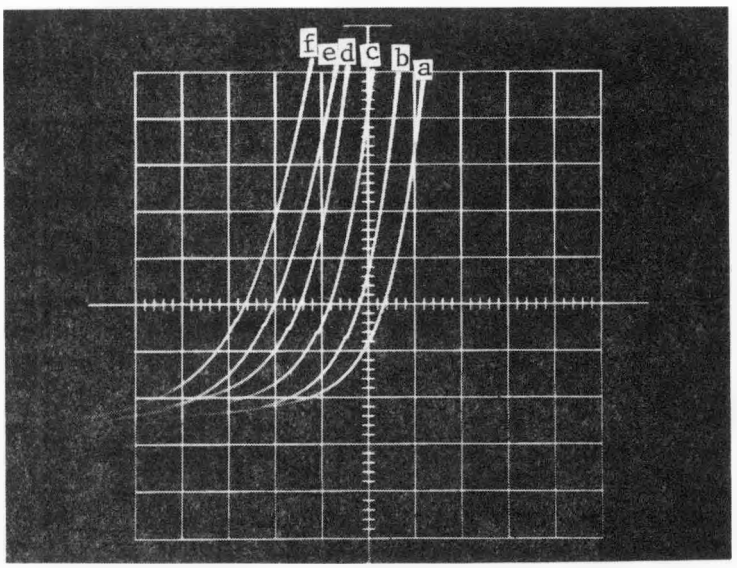

Vert = 0.1 V/div Hor = 0.1 mA/div

(Zero at Left Center of Grid)

Figure 3.7 Temperature Dependence of Open Circuit Voltage of Mg-Diffused Junction at 1 Sun Illumination; a) 25°C, b) 50°C, c) 75°C, d) 100°C, e) 125°C, and f) 150°C

When an enclosed growth system was completed, growth of Be-doped GaAsSb cells was begun. The I-V curve of one of the first Be-doped, GaAsSb bottom cells is shown in Figure 3.8. The V_{oc} for this diode is $\simeq$ 0.5 V, and J_{sc} and FF are 7.3 mA/cm^2 and $\simeq$ 0.7, respectively, yielding a 2% efficiency. The quantum efficiency was greater than 30% at the peak but dropped off very rapidly on the high energy side indicating poor minority carrier diffusion length. Further development of these diodes has yielded devices with I-V characteristics similar to that shown in Figure 3.9, which is the I-V curve of a bottom cell with a window layer and AR coating. The J_{sc} before applying the AR coating was almost 17 mA/cm^2 and increased to more than 20 mA/cm^2 and an efficiency greater than 5% with application of the coating. In fabricating this diode, the Be was diffused into the GaAsSb from the melt which was used for the AlGaAsSb window growth. Figure 3.10 and 3.11 show the spectral response and quantum efficiency, respectively. The quantum efficiency is greater than 80% over the entire frequency range to which the bottom cell must respond; this represents excellent current collection. The diode factors for good quality Be-doped junctions have been near 1.7 and have been the best measured on any antimonide samples. An EBIC scan of a diode with a window layer is shown in Figure 3.12; the Be diffused 2.5 μm during the growth of the 1 μm AlGaAsSb window layer, and the junction itself is about 2.2 μm beneath the window.

The temperature characteristics for V_{oc} of these junctions is about the same as those seen previously for the abrupt and Mg-diffused junctions, and this is shown in Figure 3.13 where the V_{oc} at 150°C is about one-half of the room temperature value.

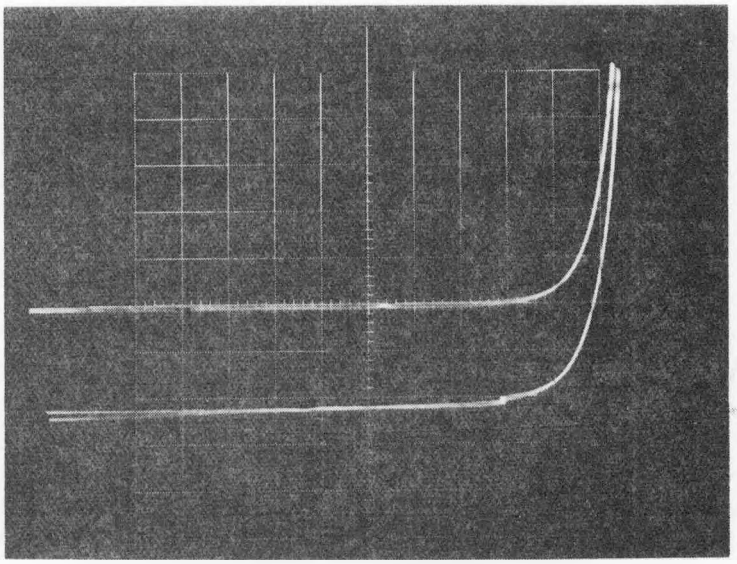

Vert = 0.02 mA/div Hor = 0.10 V/div

($V_{oc} \simeq 0.49$ V, $J_{sc} \simeq 7.3$ mA/cm^2)

Figure 3.8 I-V Curve of Early Be-Doped GaAsSb Bottom Cell (1 sun, AM0)

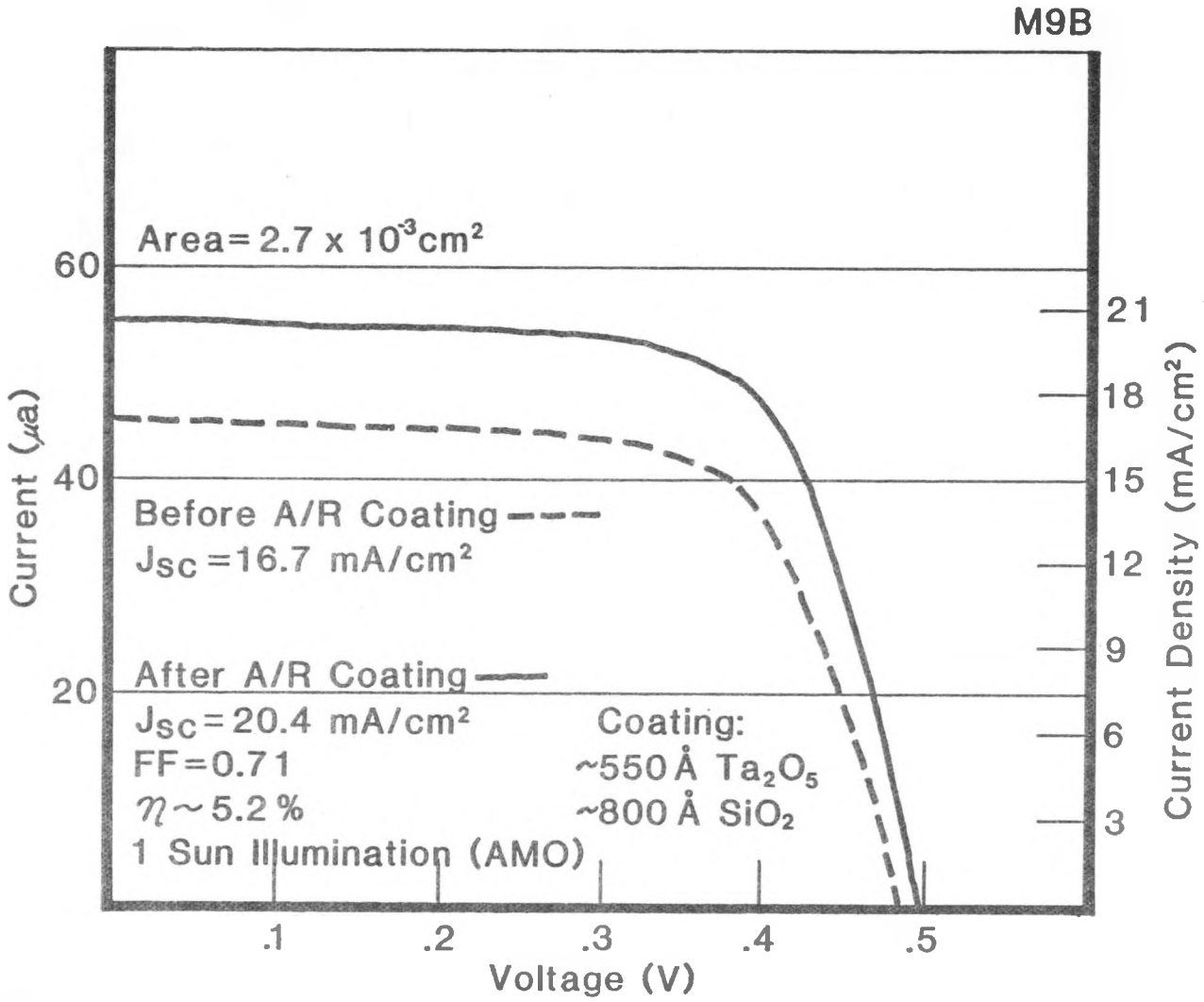

Figure 3.9 Be-Diffused, 1.2 eV GaAsSb Bottom Cell with AlGaAsSb Window Layer

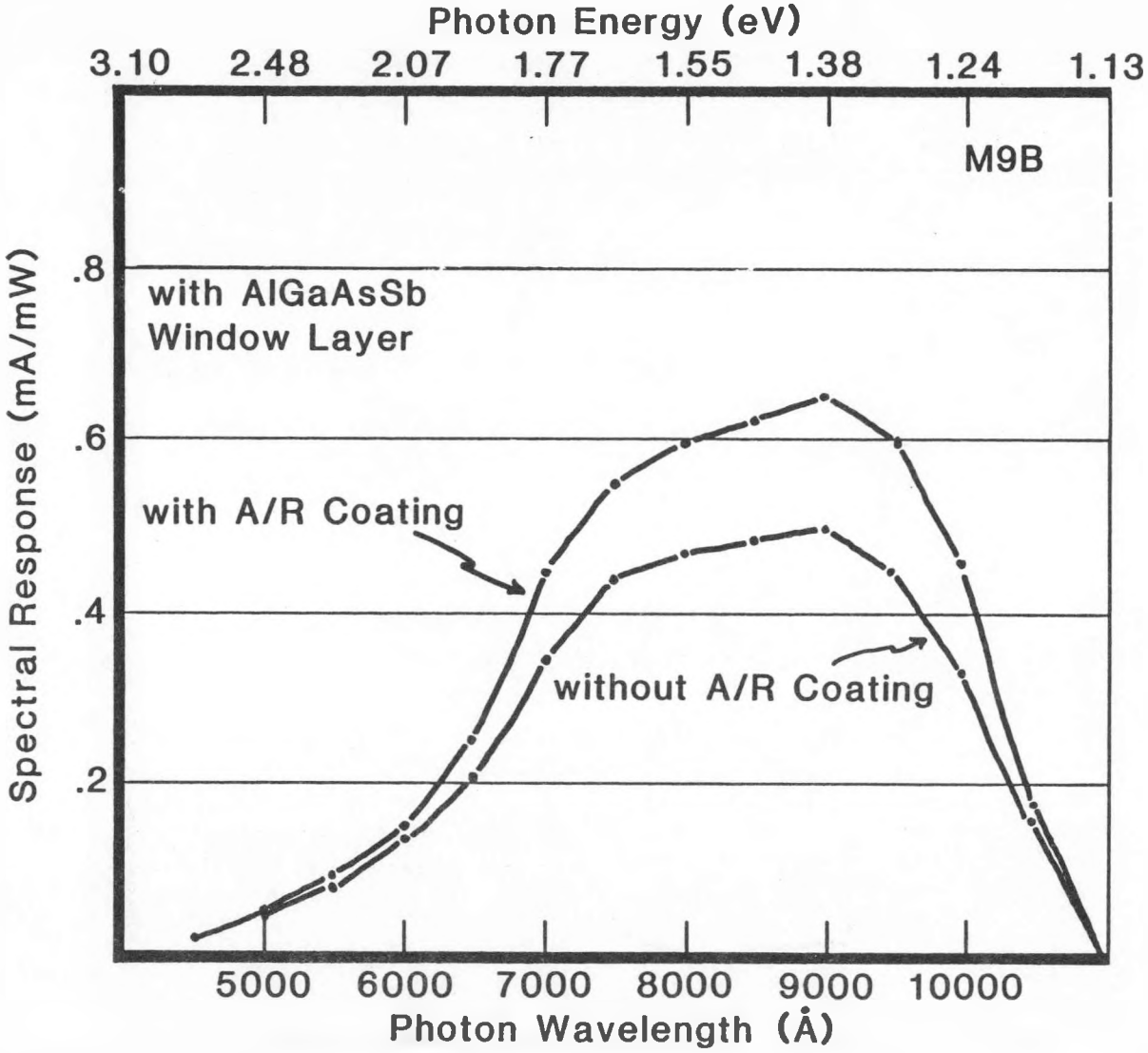

Figure 3.10 Spectral Response of 1.2 eV GaAsSb Cell (Be-Diffused Junction)

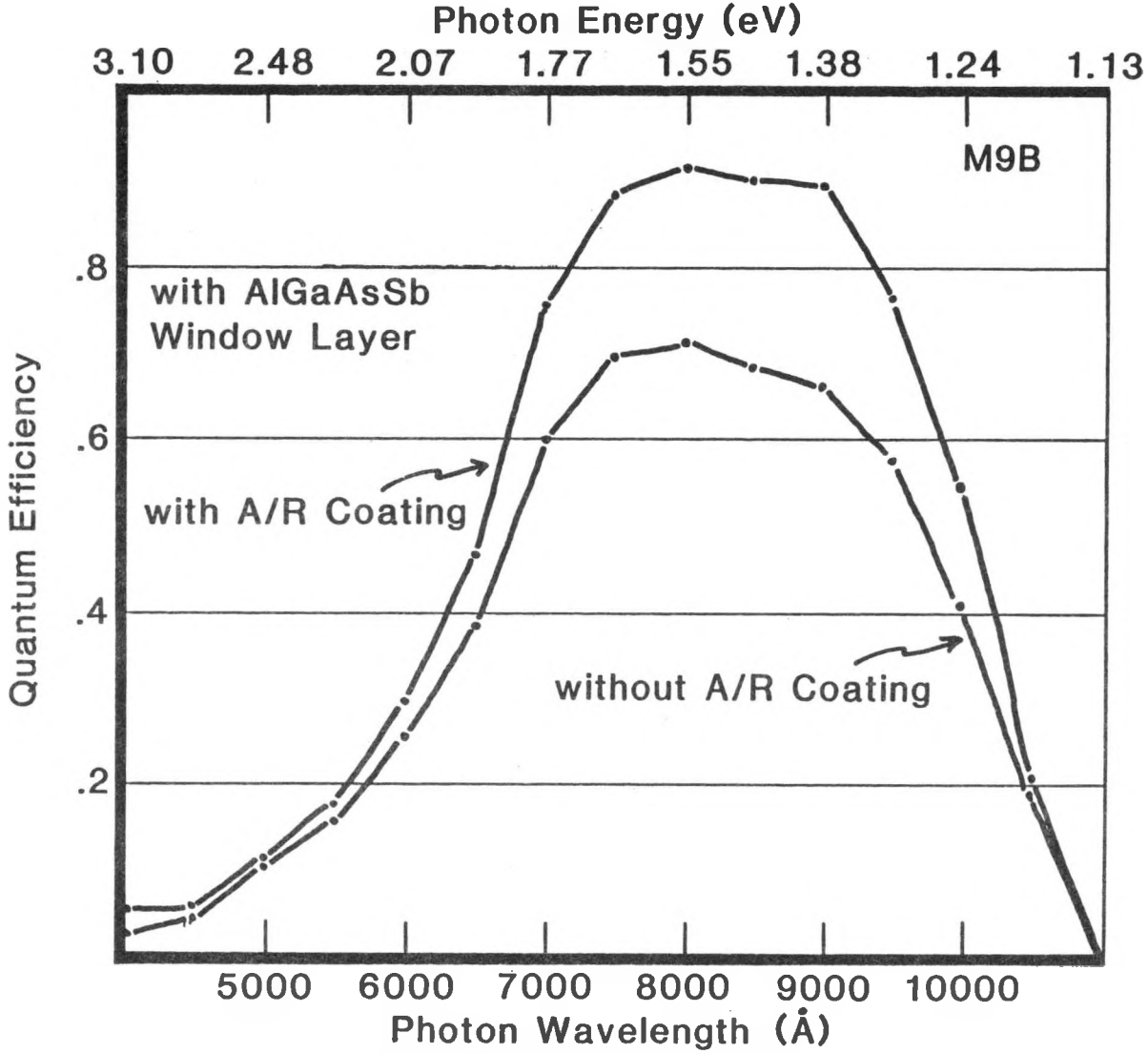

Figure 3.11 Quantum Efficiency of 1.2 eV GaAsSb Cell (Be-Diffused Junction)

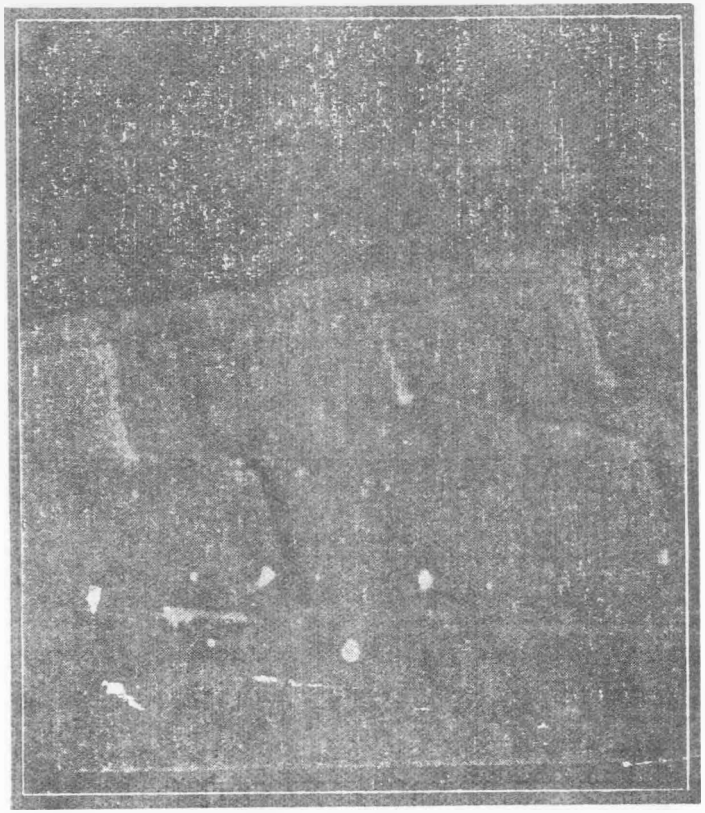

A

SEM Photomicrograph of 1.3 eV - GaAsSb Diffused Junction with 1.7 eV - AlGaAsSb Window Layer (4800 x).

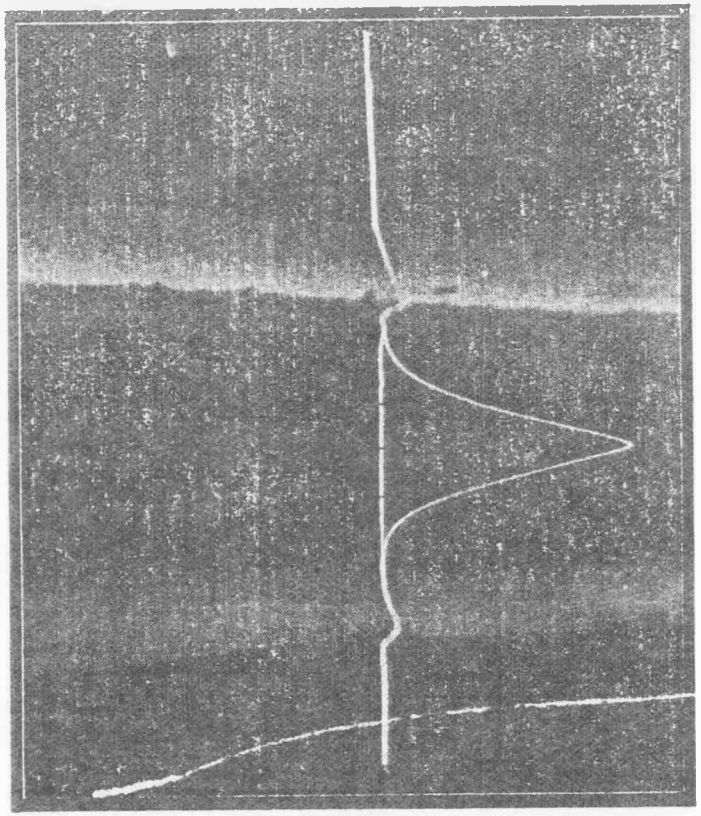

B

SEM / EBIC Scan of Diffused, 1.3 eV GaAsSb Junction with AlGaAsSb Window Layer (5000X).

Figure 3.12 EBIC Data for GaAsSb Cell

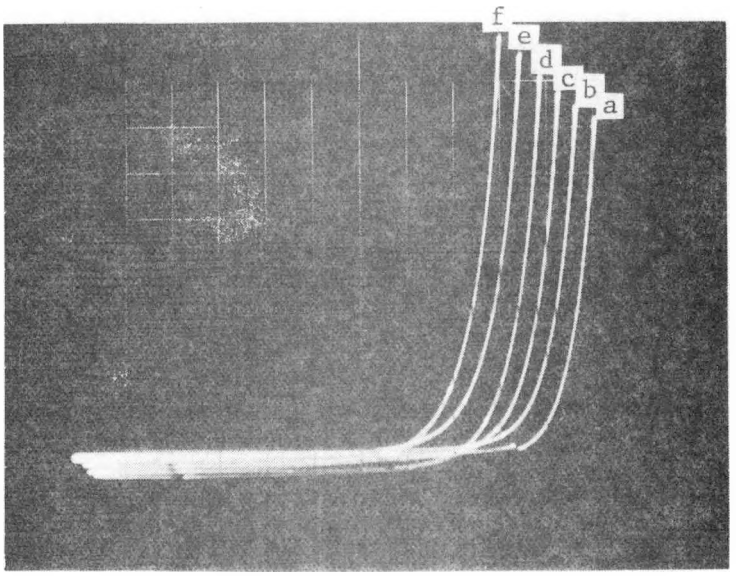

Vert = 0.02 mA/div Hor = 0.1 V/div

Figure 3.13 Temperature Dependence of Open Circuit Voltage for Be-Diffused Diode; a) 25°C, b) 50°C, c) 75°C, d) 100°C, e) 125°C, and f) 150°C

The only disappointing aspect of the Be-doped junctions was that the V_{oc} remained pinned in the vicinity of 0.5 V; it is assumed the low V_{oc} results either from the lattice mismatch mentioned earlier, from some intrinsic characteristic of antimony-containing compounds, or from an unknown defect. A similarity of experimental results in which $Ga_{0.9}In_{0.1}As$ diodes (1.27 eV bandgap) grown on GaAs (0.8% lattice mismatch) yielded V_{oc} values of 0.4 to 0.5 V has given strong support to the assumption that lattice mismatch is responsible [11].

The amount of mismatch is controlled by the concentration of Sb incorporated in the epitaxial layers (the Sb content of GaAsSb layers is, of course, dictated by the desired bandgap). If mismatch were the cause of the low V_{oc}, then reducing the Sb concentration should yield improved junction V-I characteristics. Such an experiment has been tried and the results are shown in Figure 3.14. The diode pictured is a 1.3 eV bandgap, GaAsSb layer (approx. 6% GaSb) grown directly on GaAs without the benefit of matching layers, and Be is diffused into this layer from an AlGaAsSb window. The lattice mismatch is about 0.4%, a value approximately half the mismatch between GaAs and the desired 1.2 eV GaAsSb bottom cell. The V_{oc}, J_{sc}, and FF at 1 sun (AM0) are 0.65 V, 9.4 mA/cm^2, and 0.75, respectively, and V_{oc} is equal to 0.8 V at 12 suns with very little degradation of FF. The reduced mismatch as well as the larger bandgap are believed to be responsible for these performance improvements.

The results of this experiment suggest that improved grading techniques are needed to reduce the mismatch-induced dislocation density between the bottom cell and substrate. Three such techniques that will be considered include increasing the number of step graded layers, continuous grading, and possibly superlattice grading. The last two methods would utilize MO/CVD growth techniques.

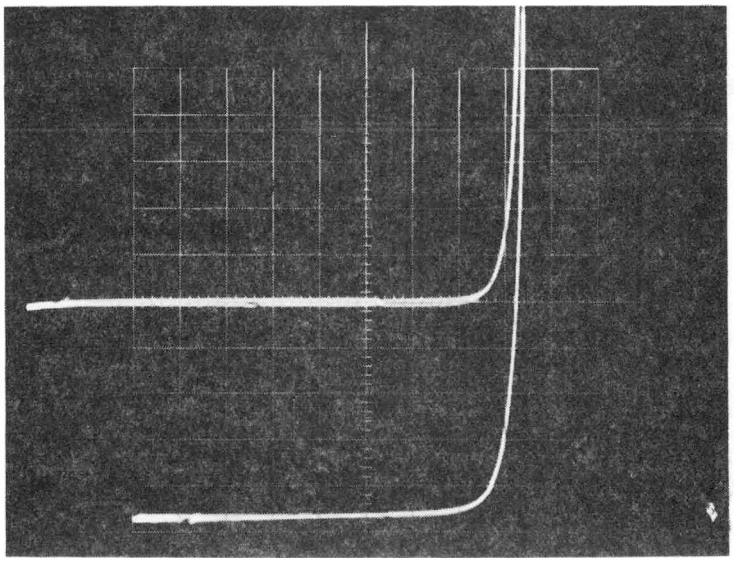

0.2 V/div
0.02 mA/div
1 sun
V_{oc} = 0.65 V
J_{sc} = 9.4 mA/cm^2

A. 1 sun

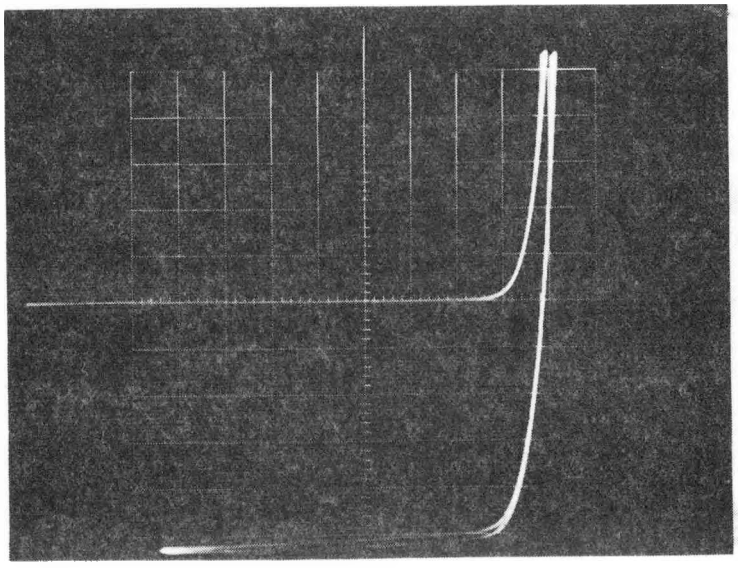

0.2 V/div
0.2 mA/div
12 suns
V_{oc} = 0.79 V
J_{sc} = 110 mA/cm^2

B. 12 suns

Figure 3.14 I-V Curves of 1.3 eV GaAsSb Diode with AlGaAsSb Window Layer but no AR Coating or Matching Layers

A comparison of Mg- and Be-doped diodes has been initiated to ascertain relative diffusion rates and performance properties of diodes. Qualitatively it can be said that FF and surface morphology appear better with Be as the dopant. The diffusion properties will be determined by the EBIC mode of SEM.

3.2 AlGaAsSb Top Cell Development

The work at developing the AlGaAsSb top cell has not been as extensive as that for ternary bottom cell, but it has followed almost an identical pattern. In initial work, Ge-doped, abrupt junctions were grown, and these junctions had low V_{oc}'s in the range of 0.55 V to 0.75 V, low J_{sc} values of 1 to 2 mA/cm^2, and FF's of 0.6 to 0.7. When Mg-diffused junctions were grown, J_{sc} generally went up to about 5 mA/cm^2, but V_{oc} remained low. Be-doped cells offered slight improvements in J_{sc} and FF.

3.2.1 Abrupt Junctions

To study top cell characteristics the Ge-doped, p-type layers of AlGaAsSb were grown on undoped, n-type layers of AlGaAsSb that had been grown on two GaAsSb matching layers. The structure is depicted in Figure 3.15 as is the I-V curve for a typical top cell. Bandgaps have ranged from ≈ 1.6 to 1.8 eV. Since the lattice parameters of the AlGaAsSb layers are about the same as the GaAsSb bottom cells, and the GaAsSb matching layers are the same composition as those used in the bottom cell research, the amount of lattice mismatch between the top cell and the GaAs substrate is about 0.8%. This high mismatch is believed to be significant in the low V_{oc} of 0.75 V (≈ 3 sun illumination)

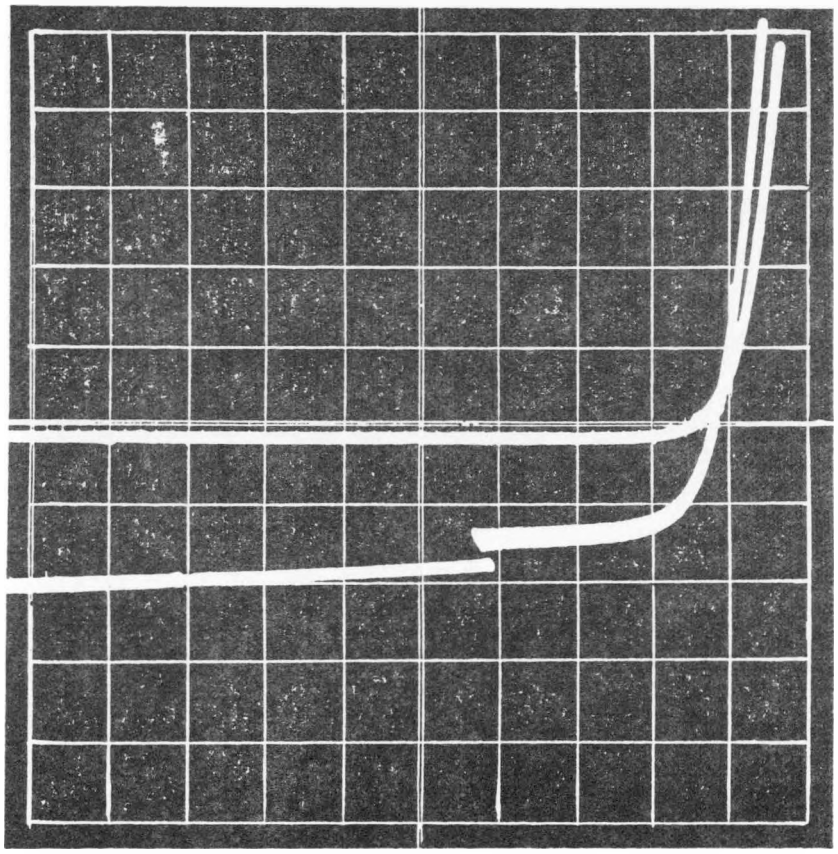

Scale
0.2 V/div
0.01 mA/div

$J_{SC} \simeq 1.2$ mA/cm^2
$V_{OC} \simeq 0.75$ V

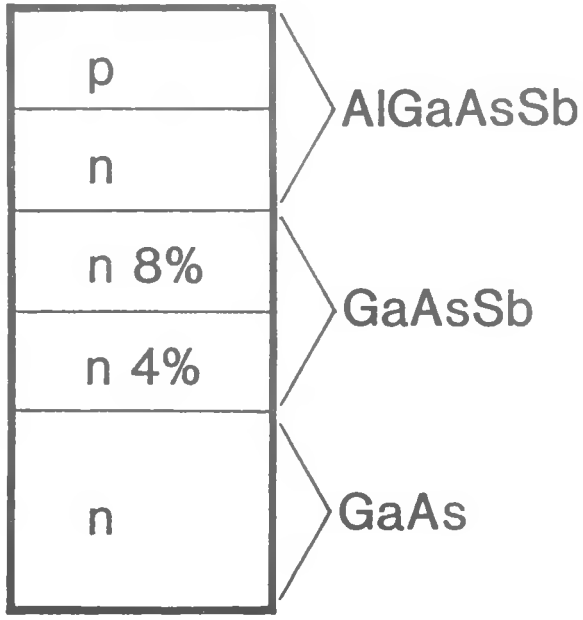

Figure 3.15 V-I Curve for GaAlAsSb Top Cell on Two Graded GaAsSb Layers

for this 1.8 eV diode. Also indicated in Figure 3.15 is a low J_{sc} of 1.2 mA/cm^2. This value is quite typical for most of the abrupt junctions that were grown, and most of the V_{oc} measurements gave values less than 0.75 V. The FF values are generally near 0.65, and efficiencies are quite poor (less than 1%). The quantum efficiencies are poor also.

While the poor device performance is attributed to lattice mismatch and interface phenomena of the abrupt junction, there are other complexities in growing AlGaAsSb. First, the growth rate is much slower for the quaternary than the ternary. GaAsSb grows about 0.8 μm per degree of cooling (at ≃ 780-800°C), and AlGaAsSb grows almost an order of magnitude more slowly at 0.08 to 0.12 μm per degree during near-equilibrium growth.

Second, in our work, the addition of Al has been found to reduce the amount of Sb incorporated into the solid at the growth temperature (800°C) and to reduce the As solubility in the melt. The former result is contrary to what has been reported by Antypas and Moon [12] who noted essentially constant Sb composition for AlGaAsSb growth above 760°C. The ramification is that care must be taken in melt preparation when differing amounts of Al are involved; this is done with the cascade structure to insure that lattice matching exists among the various layers.

Third, by having a slow growth rate, fairly large temperature drops must be used to grow even modestly thin layers. This can result in high degrees of supersaturation for subsequent melts and spontaneous nucleation of AlGaAsSb crystallites. This is believed to cause the macroscopic hillocks which have been noted in the surface morphology of most of the grown layers. Efforts to control this degree

of supersaturation by limiting the As available to the melt have resulted in better surface morphologies with very bright shiny layers and fewer hillocks.

3.2.2 Diffused Junctions

Mg-diffused junctions have shown substantial increases in J_{sc} and quantum efficiency. The I-V curve of a typical 1.8 eV bandgap junction is shown in Figure 3.16 at 1 sun (AM0) illumination; V_{oc}, J_{sc}, and FF are equal to 0.65 V, 6.3 mA/cm^2, and 0.68, respectively. The efficiency of this junction, which has an AR coating, is greater than 2%; the peak quantum efficiency is greater than 20% and the diode factor is about 1.9.

Be-diffused junctions have also been grown, and the I-V curve for a sample (1.55 eV bandgap with an AlGaAsSb window) is shown in Figure 3.17. J_{sc} was almost 7 mA/cm^2 before application of the AR coating, and it rose to 8 mA/cm^2 after coating application, a 19% increase. V_{oc} is low at 0.55 V, but the efficiency is still more than 2%. In Figures 3.18 and 3.19 spectral response and quantum efficiency data are presented. The peak quantum efficiency is greater than 60% but has an extremely rapid falloff on the high energy side. This high energy falloff is much more severe than was observed for the GaAsSb cells and indicates a considerably shorter minority carrier diffusion length for the quaternary than the ternary.

V_{oc} decreases in AlGaAsSb top cells with increasing temperature at almost the same rate as in GaAsSb bottom cells; an example of this decrease is shown in Figure 3.20. At 150°C, V_{oc} is between 50 and 60% of the room temperature value. J_{sc} (150°C) is about 8 to 10% higher than J_{sc} (25°C).

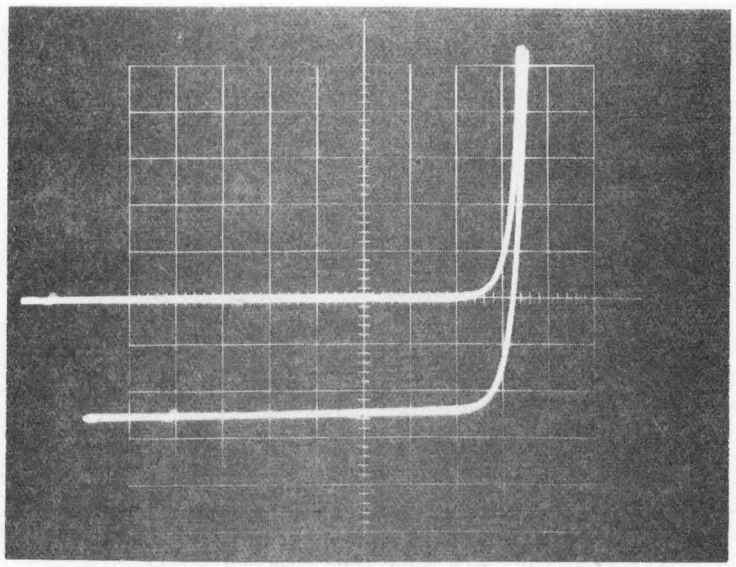

Vert = 0.02 mA/div Hor = 0.2 V/div

($V_{oc} \simeq 0.65$ V, $J_{sc} \simeq 6.3$ mA/cm^2)

Figure 3.16 I-V Curve of Mg-Diffused Top Cell with AR Coating (1 sun, AM0)

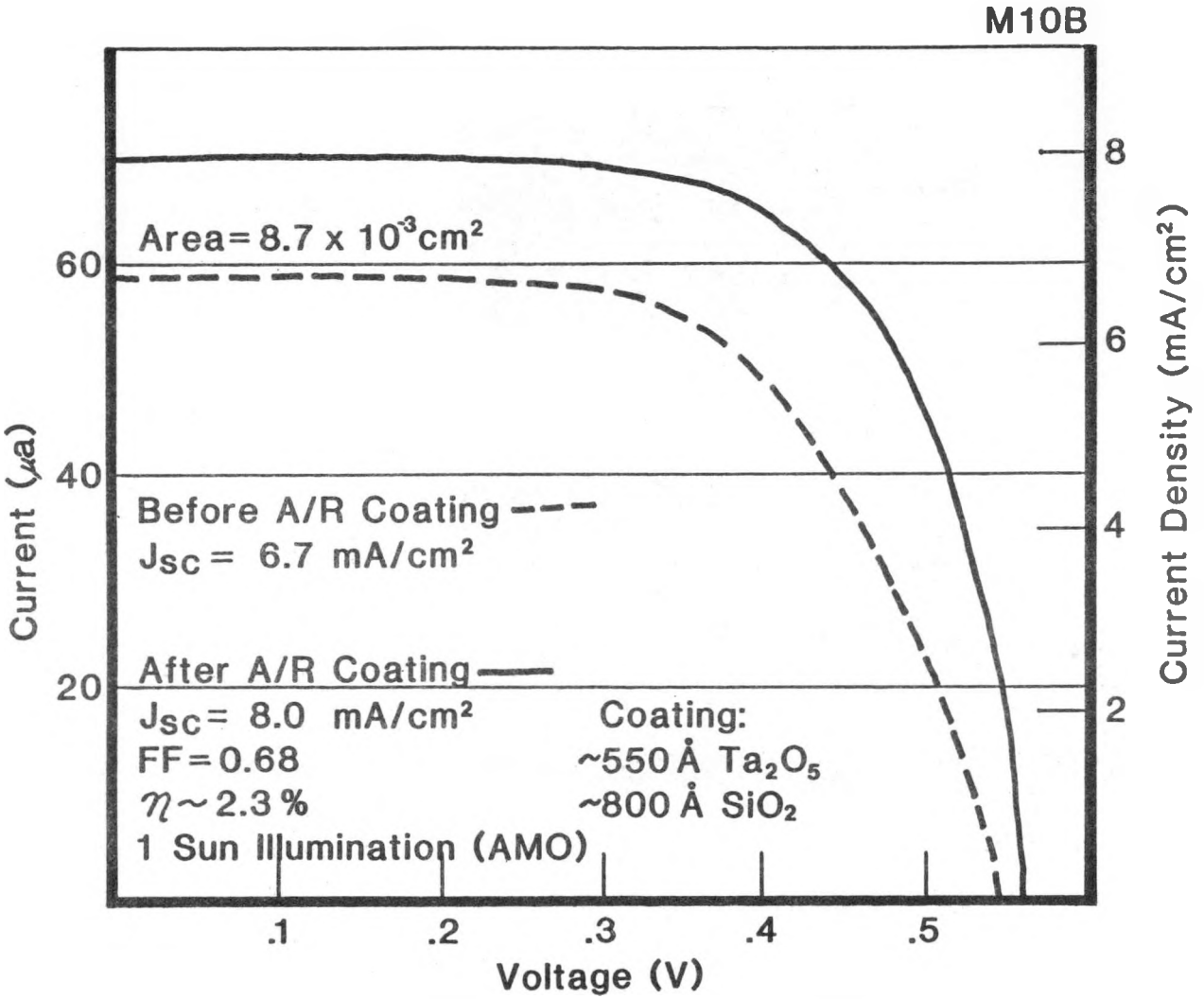

Figure 3.17 Be-Diffused, 1.55 eV AlGaAsSb Top Cell with AlGaAsSb Window Layer

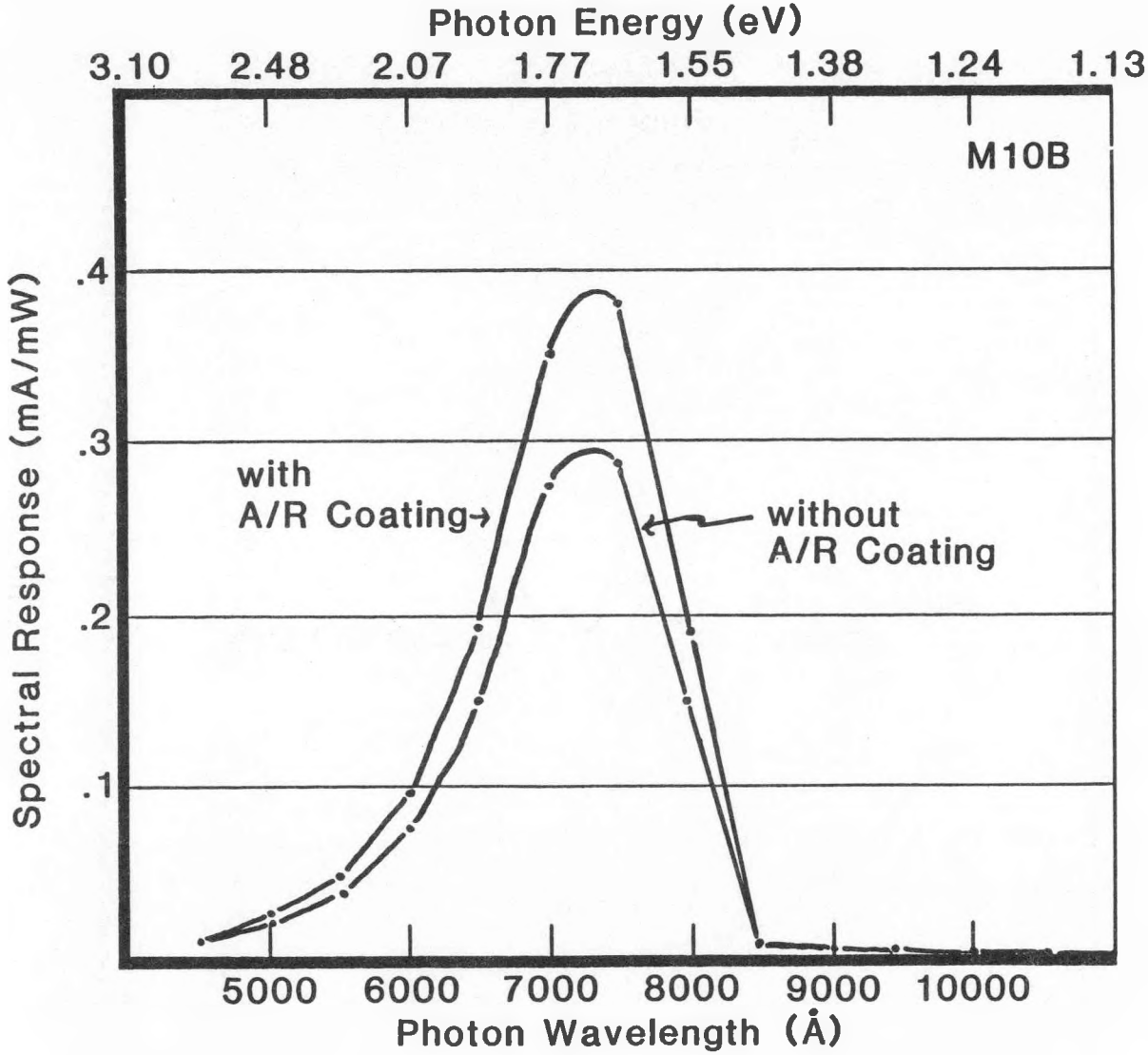

Figure 3.18 Spectral Response of 1.55 eV AlGaAsSb Cell (Be-Diffused Junction) with AlGaAsSb Window Layer

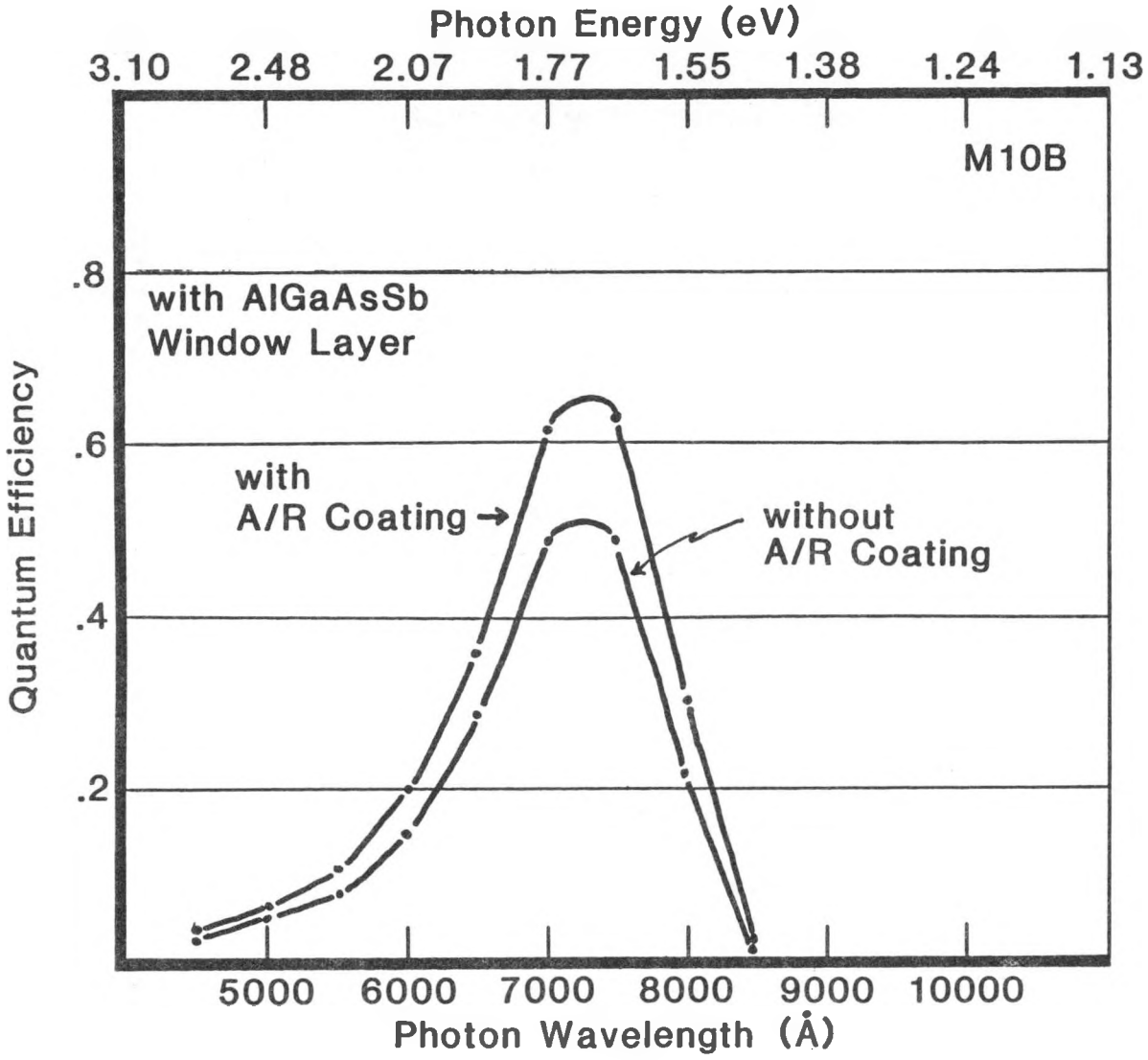

Figure 3.19 Quantum Efficiency of 1.55 eV AlGaAsSb Cell (Be-Diffused Junction) with AlGaAsSb Window Layer

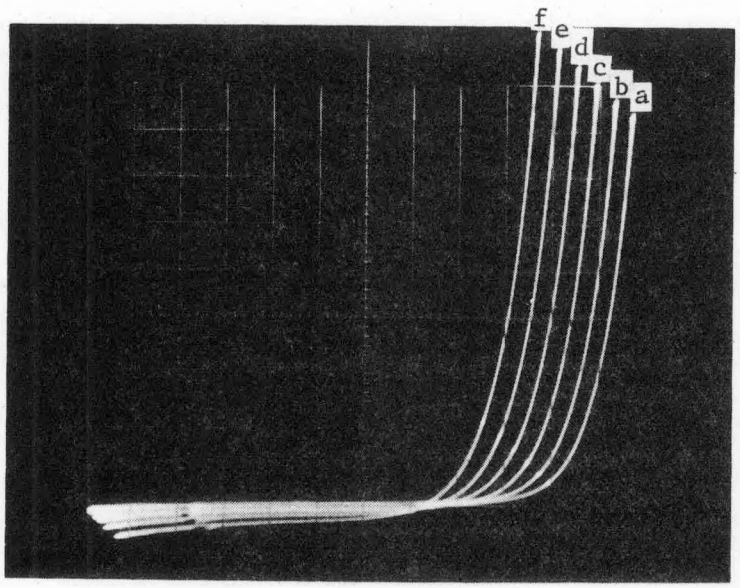

Vert = 0.02 mA/div Hor = 0.1 V/div

Figure 3.20 Temperature Dependence of Open Circuit Voltage; a) 25°C, b) 50°C, c) 75°C, d) 100°C, e) 125°C, and f) 150°C

3.3 Cascade Cell and Tunnel Junction Development

Two different configurations have been developed for the AlGaAsSb/GaAsSb cascade cell--one employing abrupt junctions and the other diffused junctions. These configurations are depicted in Figure 3.21.

Abrupt junction cascade cells (Fig. 3.21a) have been fabricated and were described in a previous annual report [6]. Although fabrication of these structures has continued, problems manifested by low V_{oc} and J_{sc} have continued with this configuration. Typical I-V data for an experimental device are shown in Figure 3.22.

I-V characteristics at elevated temperatures have also been measured for abrupt-junction cascade cells as illustrated in Figure 3.23. V_{oc} decreases from 1 V (1 sun, AM0) at 25°C to slightly less than 0.5 V at 150°C. I_{sc} increased from 0.025 mA to between 0.035 and 0.040 mA for the same temperature range, while the FF degraded significantly. These temperature characteristics are almost identical to those of individual junctions, both abrupt and diffused.

Improvements realized in the performance of individual cells grown separately using diffusion techniques suggest that cascade structures employing diffused junctions should be superior to those using abrupt junctions. In the diffused junction cell of Figure 3.21b, the bottom and top cells are diffused from the p+ layers of the tunnel junction and the window, respectively, two grown layers. An alternative which has worked well for the AlGaAs/GaAs cells is to introduce a p+ window layer between the p+ layer of the tunnel junction and the n-type layer of the bottom cell; the bottom cell is diffused from this window, and the two stacked p+ layers make upward diffusion from the window layer a less severe problem. Even with this alternate scheme, one less layer is required.

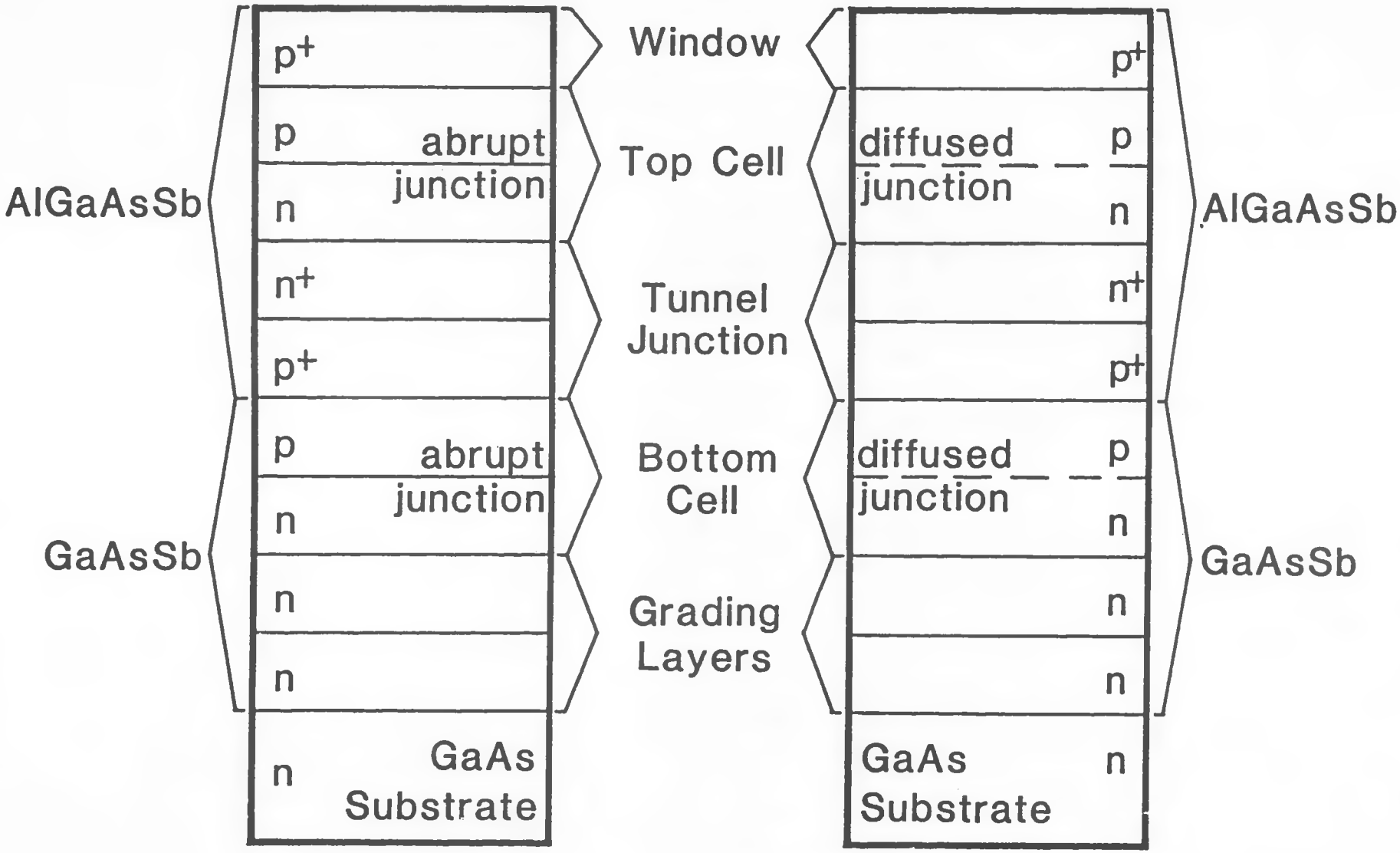

A. 9 Layer
Abrupt Junction Structure

B. 7 Layer
Diffused Junction Structure

Figure 3.21 GaAlAsSb/GaAsSb Cascade Structures

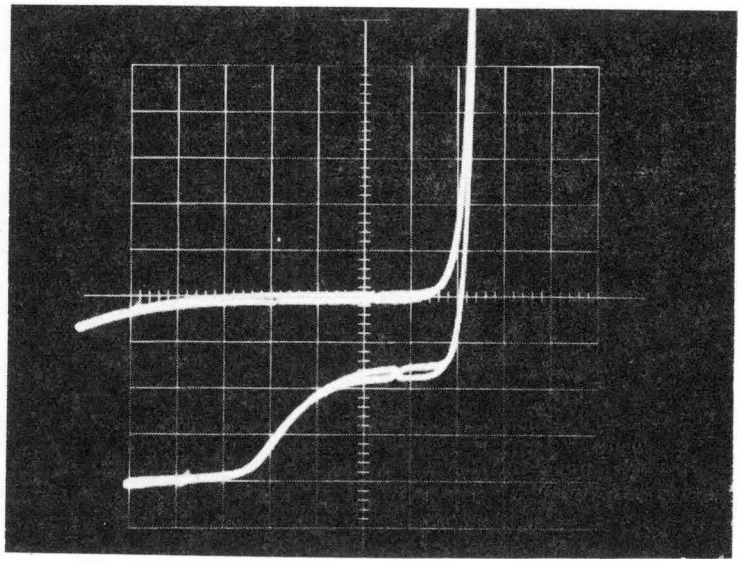

Vert = 0.01 mA/div Hor = 0.5 V/div

Figure 3.22 I-V Curve of Abrupt Junction Cascade Cell Showing No Tunnel Junction Interferences

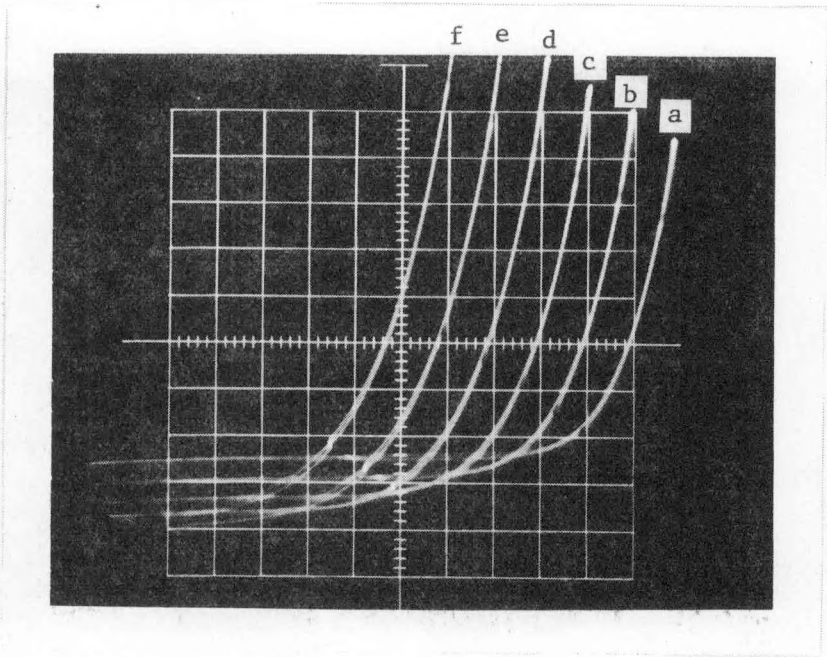

Vert = 0.01 mA/div Hor = 0.1 V/div

Figure 3.23 Open Circuit Voltage Dependence on Temperature:
a) 25°C, b) 50°C, c) 75°C, d) 100°C, e) 125°C, f) 150°C

Note: Origin at Center of Left Axis

Attempts to grow the cascade cells using diffused junctions have not been markedly successful to date. There have been two major problems, tunnel junction interference and shorted top cells. Tunnel junction interference manifests itself in one of two ways usually: either there is a problem with nonlinear resistance which greatly degrades the FF as shown in Figure 3.24, or the backward diode characteristic, superimposed on the cells I-V characteristic, affects J_{sc} and V_{oc} as shown in Figure 3.25. For these structures, Mg was used to dope the tunnel junction and diffuse the bottom cell p-type layer, but it also apparently diffuses into the n+ layer of the tunnel junction, thereby compensating this layer and increasing its resistivity or yielding a backward diode.

To avoid the diffusion problems mentioned above, the cooling rate was increased during growth; however, in most runs top cells have either been shorted or have failed to grow uniformily across the substrate. The bottom cells in these structures having shorted top junctions performed well with some current densities reaching nearly 20 mA/cm^2.

Even when the top cells were not shorted, they usually limited J_{sc} of the cascade structure. This is demonstrated in Figure 3.26 which shows the I-V curve of a cell (Mg-diffused junctions) illuminated with a xenon lamp and with xenon plus tunsten lamps. The tunsten has a spectral content containing photons with a lower average energy, so the bottom cell should respond more strongly. This is evident in Figure 3.25, and provides confirmation that the top cell is limiting J_{sc}.

3.4 Future Improvements

In order to improve the surface morphology of grown layers, two twelve-well graphite boats have been procured and placed into operation.

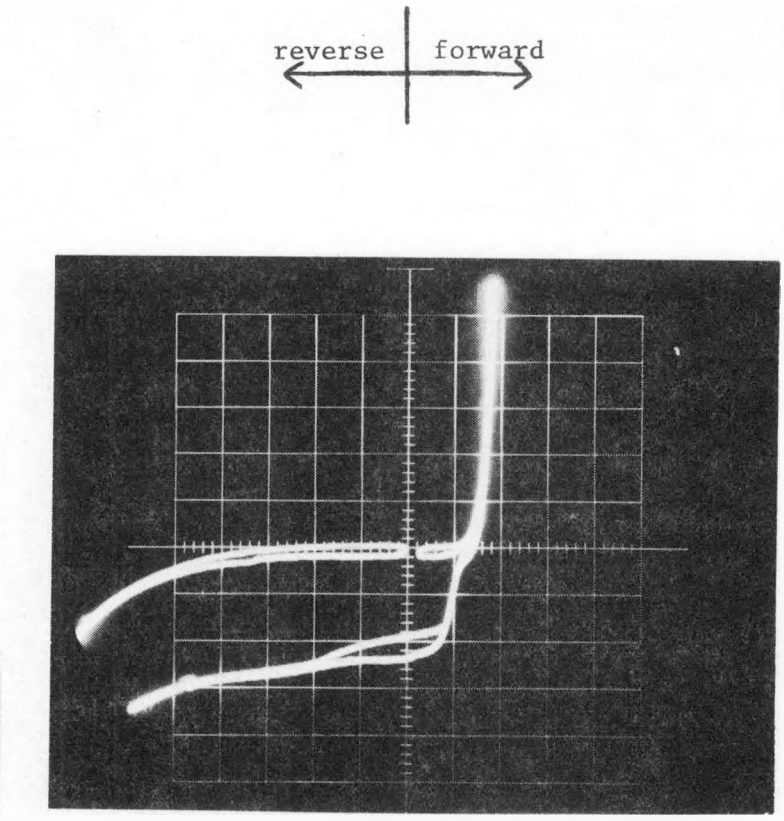

Vert = 0.2 mA/div Hor = 1.0 V/div

Figure 3.24 I-V Curve of Cascade Cell Showing Nonlinear Resistance Effects from Tunnel Junction

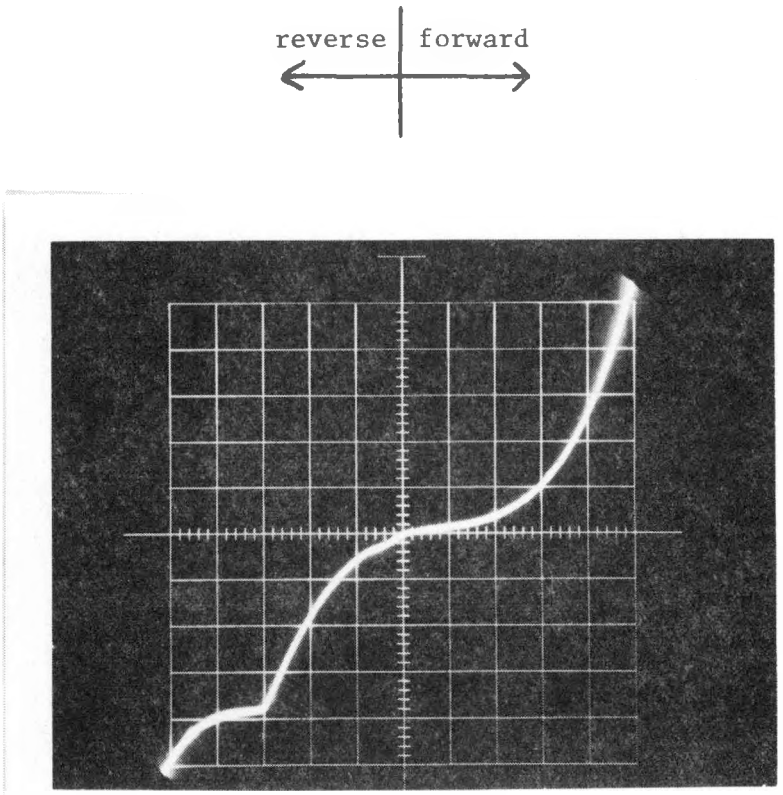

Vert = 0.5 mA/div Hor = 2.0 V/div

Figure 3.25 I-V Curve of Cascade Cell with Tunnel Junction Behaving as Backward Diode

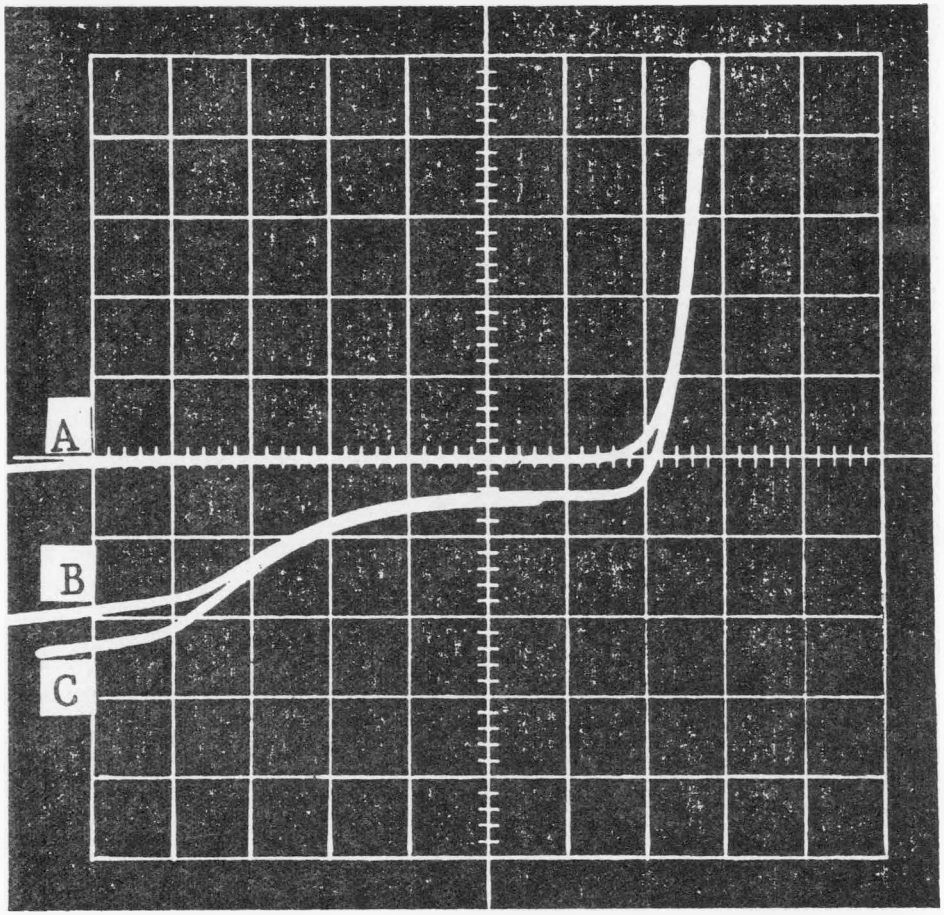

Scale
Vert. 0.05 mA/div
Horiz. 0.5 V/div

A. Dark Curve

B. Illumination from Xenon Lamp

C. Illumination from Xenon Lamp and Tungsten Lamp

Figure 3.26 Effect of Light Source on AlGaAsSb/GaAsSb Cascade Solar Cell

From a design point of view, the only difference between these boats and those currently in use is that the spacing between the wells is 0.1 in. instead of 0.5 in. This results in substrates being uncovered while between melts for much shorter time periods during the growth sequence; this has resulted in improved GaAsSb surface morphology in this work and is consistent with results reported elsewhere [13]. Surface morphologies have consistently been good for GaAsSb and for AlGaAsSb when control of the degree of supersaturation is exercised. Figure 3.27 shows a cleaved, stained sample which has ten GaAsSb layers, while Figure 3.28 shows the surface of an AlGaAsSb layer; both layers were grown with the new boat. Note that there are very few of the hillocks which have been so prevalent in the AlGaAsSb growth. The twelve-well boat also offers wider growth flexibility and will permit an increased number of graded layers. It is hoped that this new boat will result in improved quality ternary and quaternary layers, and thereby eliminate difficulties currently being experienced with the diffused junction cascade structures. Other approaches that will be considered to improve this cascade structure include the use of continuous grading between substrate and bottom cell and, possibly, superlattice grading as mentioned in Section 3.1.2.

3.5 Summary

The most important developments in the past year have been the growth of GaAsSb and AlGaAsSb diodes with diffused junctions. Both Mg and Be have served as the p-type diffusing specie in these structures and considerable improvements in J_{sc} were recorded with values greater than 20 mA/cm^2 and about 8 mA/cm^2 for bottom and top cells, respectively. These results were measured on cells which had been grown separately and

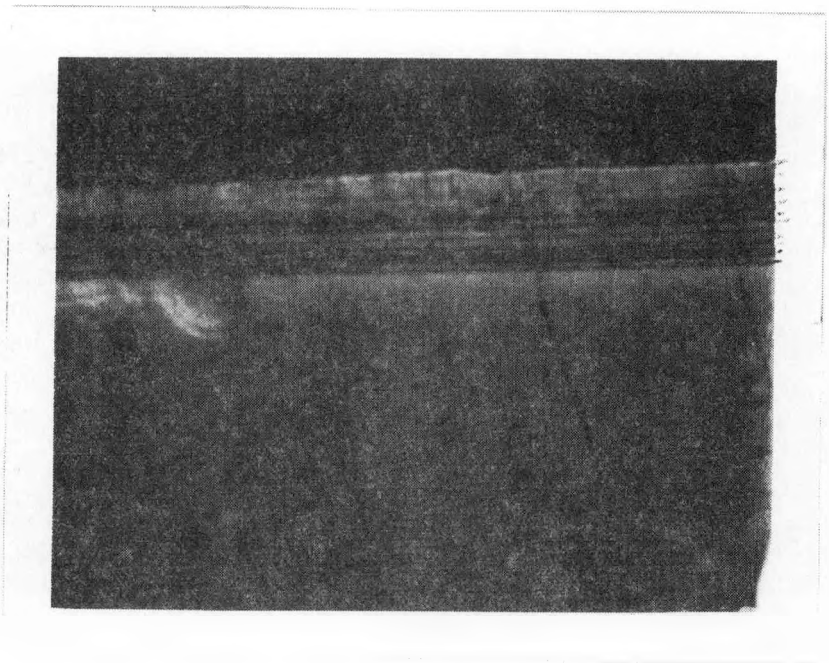

Figure 3.27 Cleaved, Stained Cross-Section of Ten Layer GaAsSb Structure (910x). Layer Composition Increased from $GaAs_{0.98}Sb_{0.02}$ to $GaAs_{0.88}Sb_{0.12}$. Last Four Layers Have Same Composition.

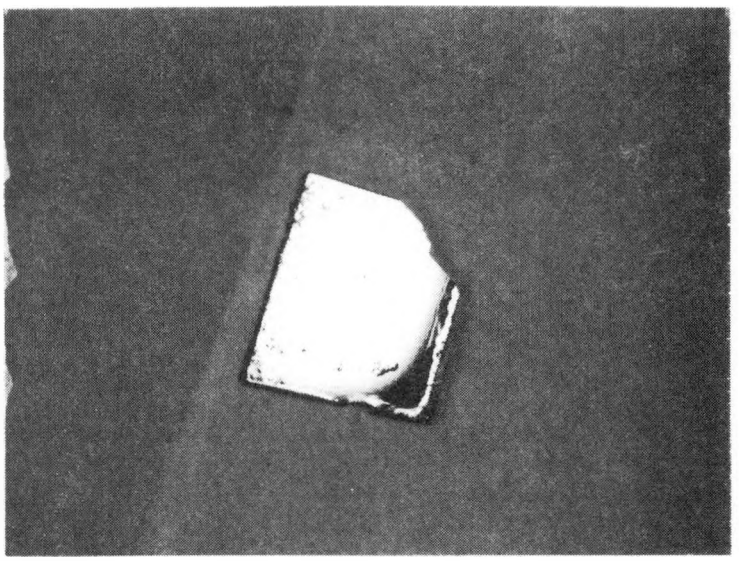

Figure 3.28 AlGaAsSb Layer Grown on GaAs. Supersaturation Has Been Controlled and Only a Few Hillocks are Visible.

which had both window layers and AR coatings. Separating the metallurgical and electrical junctions is believed to be the reason for the improved carrier collection. Peak quantum efficiencies greater than 90% for bottom cells have been measured indicating the efficient current collection.

Similar improvements have not been seen with the V_{oc} problem. V_{oc}'s have remained low--0.45 to 0.55 V for bottom cells and 0.6 to 0.7 V for top cells (1 sun, AM0)--regardless of the junction type. This has been attributed to dislocations resulting from the 0.8% lattice mismatch between the substrate and the GaAsSb bottom cell. Diode factors for the diffused junction are slightly lower than those of abrupt junctions--1.7 to 1.8 as compared to $\simeq$ 2--but current is still being controlled by depletion region recombination. The low V_{oc} remains the most critical problem with AlGaAsSb/GaAsSb cell research.

The successes of diffused junctions with single junction cells has led to initial efforts to fabricate cascade structures having diffused junctions. Such structures are simpler, requiring less layers and should be capable of higher efficiencies due to improved J_{sc} and V_{oc}.

The V_{oc} vs. temperature characteristics of cascade and separately grown top and bottom cells continue to be monitored. Thus far, it appears that V_{oc} at 150°C is between 50 and 60% of that at room temperature. This apparently is true for abrupt and diffused top and bottom cells and for cascade cells with abrupt junctions.

Finally, the effectiveness of the two-layered AR coating ($\simeq$ 550 Å of Ta_2O_5 and $\simeq$ 800 Å of SiO_2) has been demonstrated. J_{sc} increases on the order of 20 to 25% are typical. It should be noted that this coating has not been rigorously optimized for the antimonide cell although it does appear quite effective.

4.0 ORGANOMETALLIC-CHEMICAL VAPOR DEPOSITION RESEARCH

The overall objective of this work is to explore the feasibility of using the OM/CVD growth technique for the fabrication of various parts of the cascade solar cell structure. Since the OM/CVD technique is not as well developed and characterized as the LPE technique, much of this research has been directed toward understanding and characterizing the OM/CVD growth process.

4.1 GaAs Growth

GaAs has been grown and characterized periodically to determine the quality of the material being grown with the OM/CVD equipment. The best undoped layers have been p-type with a background concentration of around $5 \times 10^{15} cm^{-3}$ and a Hall mobility of approximately 260 cm^2/V sec. N-type doping has been accomplished with Te from dimethyltelluride; Hall data for two samples at $1.4 \times 10^{17} cm^{-3}$ and at $2.4 \times 10^{18} cm^{-3}$ are shown in Figure 4.1.

Photoluminescence has been measured on the OM/CVD GaAs material and the results are shown in Figure 4.2. The photoluminescence peak was found to occur at $\lambda/2 = 4420$ Å at room temperature, corresponding to an energy of 1.403 eV. Measurements on the GaAs substrate material give photoluminescence results with a peak intensity about twice that of the OM/CVD material and with a half width approximately the same as that of the OM/CVD material. However, the emission peak of the substrate material occurs at 1.412 eV or about 9 meV above that of the OM/CVD material. The exact reason for this is not known. The difference may be due to different shallow impurity species in the substrate and the OM/CVD material.

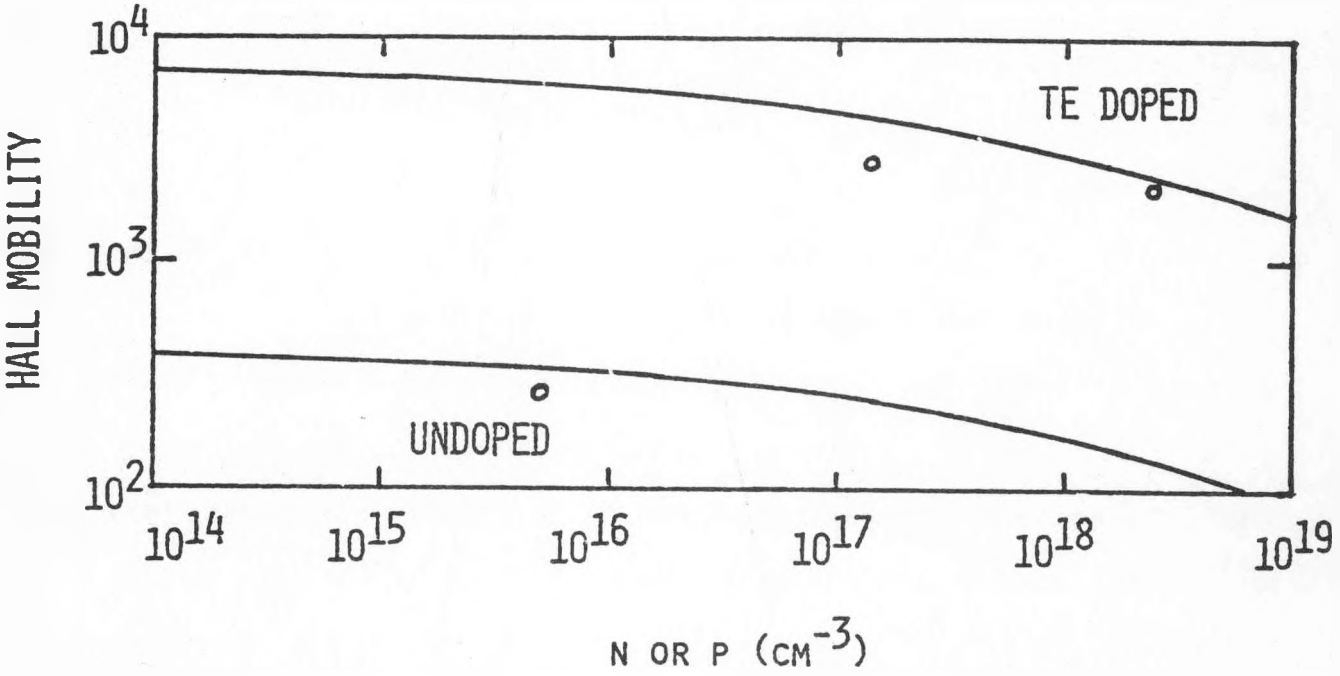

Figure 4.1 Hall Mobility Data for Undoped and Te Doped GaAs Samples. The Solid Curves are from Sze.

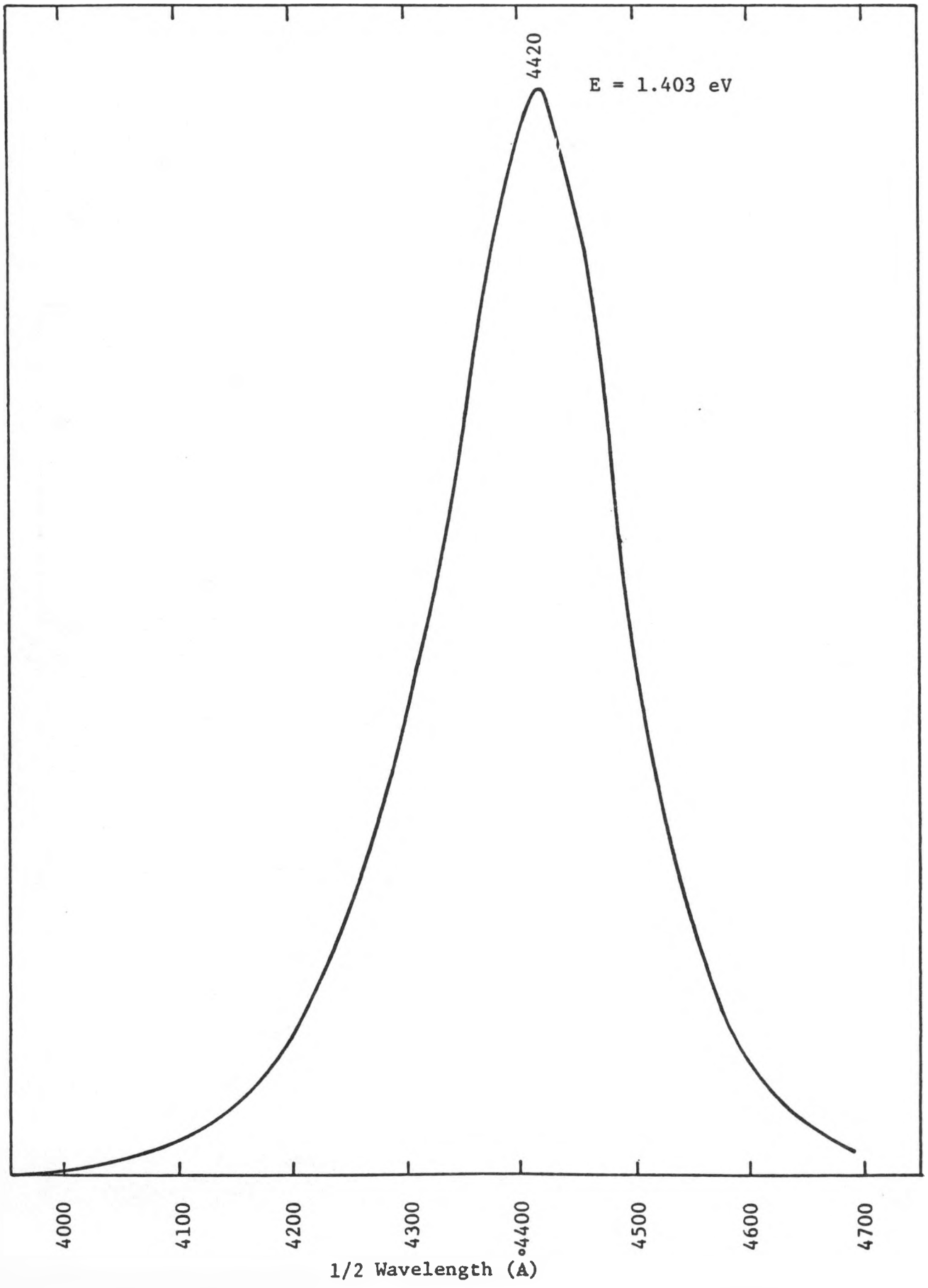

Figure 4.2 Photoluminescence of OM-CVD GaAs (Room Temperature)

4.2 AlGaAs Growth

Considerable effort was spent on the OM-CVD growth of AlGaAs for potential use in an AlGaAs/GaInAs cascade solar cell. It was decided during the last quarter of this contract to terminate this approach in favor of the lattice-matched AlGaAsSb/GaAsSb cell. However, this work is reported here for completeness in summarizing the work undertaken during this contract period.

Characterization of the AlGaAs growth process was one of the major activities. The most important growth parameters appear to be the TMAl to TMGa flow ratio and the total AsH_3 flow rate. For a constant AsH_3 flow rate, Figure 4.3 shows the AlAs composition as a function of the flow ratio of hydrogen through the TMAl bubbler at 20°C and the TMGa bubbler at 0°C. The composition was determined from microprobe data. Figure 4.4 shows that there is an interaction between the achieved AlAs composition and the total AsH_3 flow rate. At a constant ratio of TMAl to TMGa transport, Figure 4.4 shows a decrease in AlAs composition from about 52% to about 33% as the AsH_3 (5% in H_2) flow rate increases from 100 cc/min to 175 cc/min. Large AsH_3 flow rates appear to suppress the AlAs composition.

The conditions required for the growth of desired layers of AlGaAs now appear to be pretty well characterized.

Carrier densities have been measured on several samples by use of Schottky barriers and the C-V technique. Figure 4.5 shows the I-V characteristic of an Au Schottky barrier of 15 mils in diameter on a sample with about 20% AlAs. Figure 4.6 shows the corresponding capacitance data for such a sample, indicating a background n-type doping density of $2.5\text{-}5.7 \times 10^{15} cm^{-3}$. Several other GaAlAs samples have given

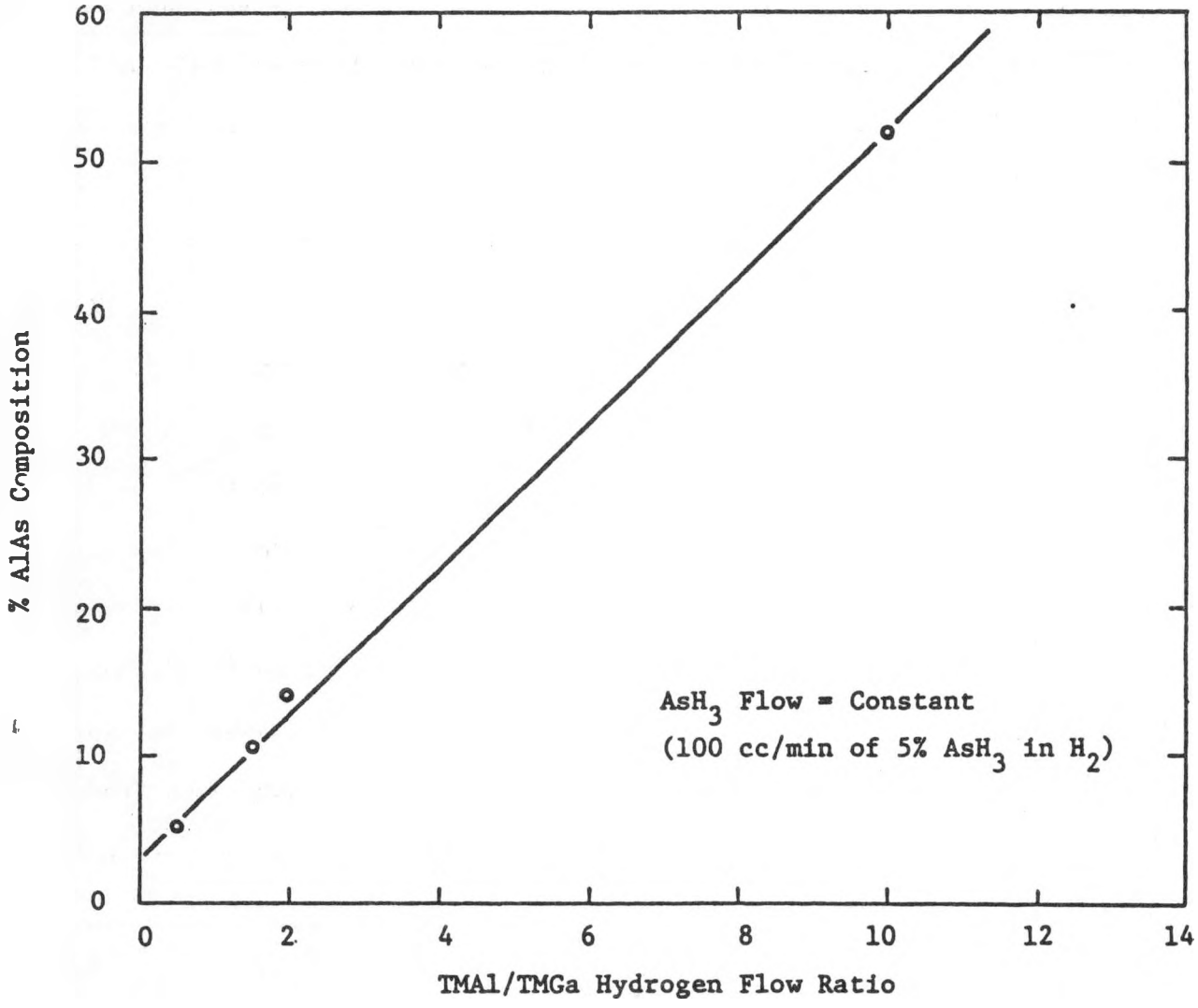

Figure 4.3 AlAs Composition for Varying Ratios of TMAl to TMGa

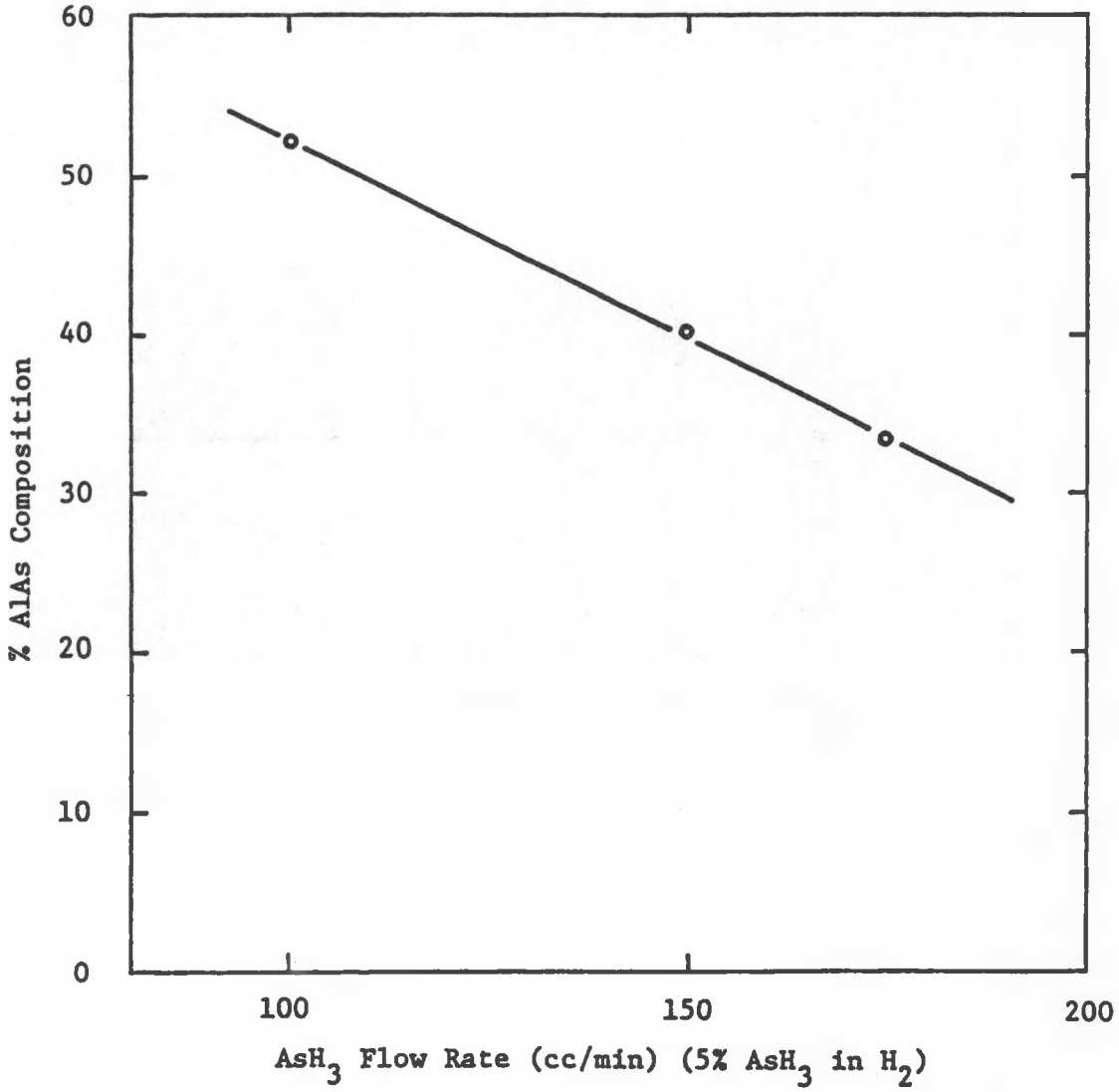

Figure 4.4 Effect of AsH_3 Flow on AlAs Composition

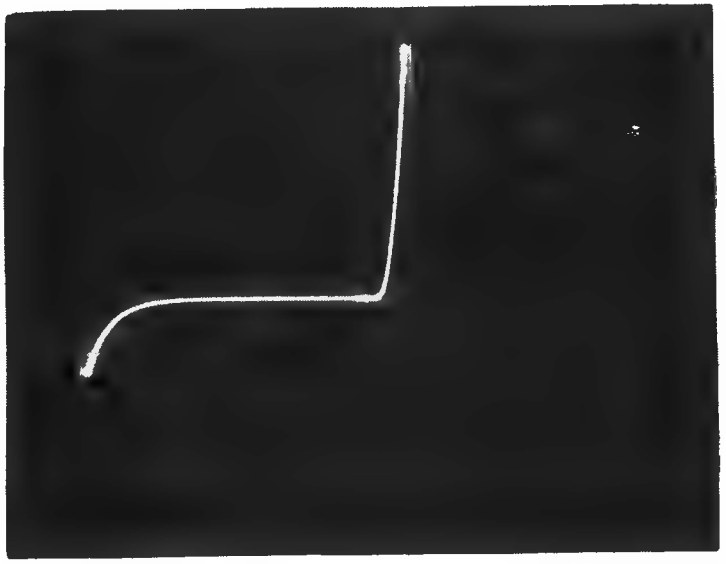

Figure 4.5 I-V Characteristic of Schottky Diode on AlGaAs Layer.
Scale: 0.1 mA/div, 1.0 V/div.

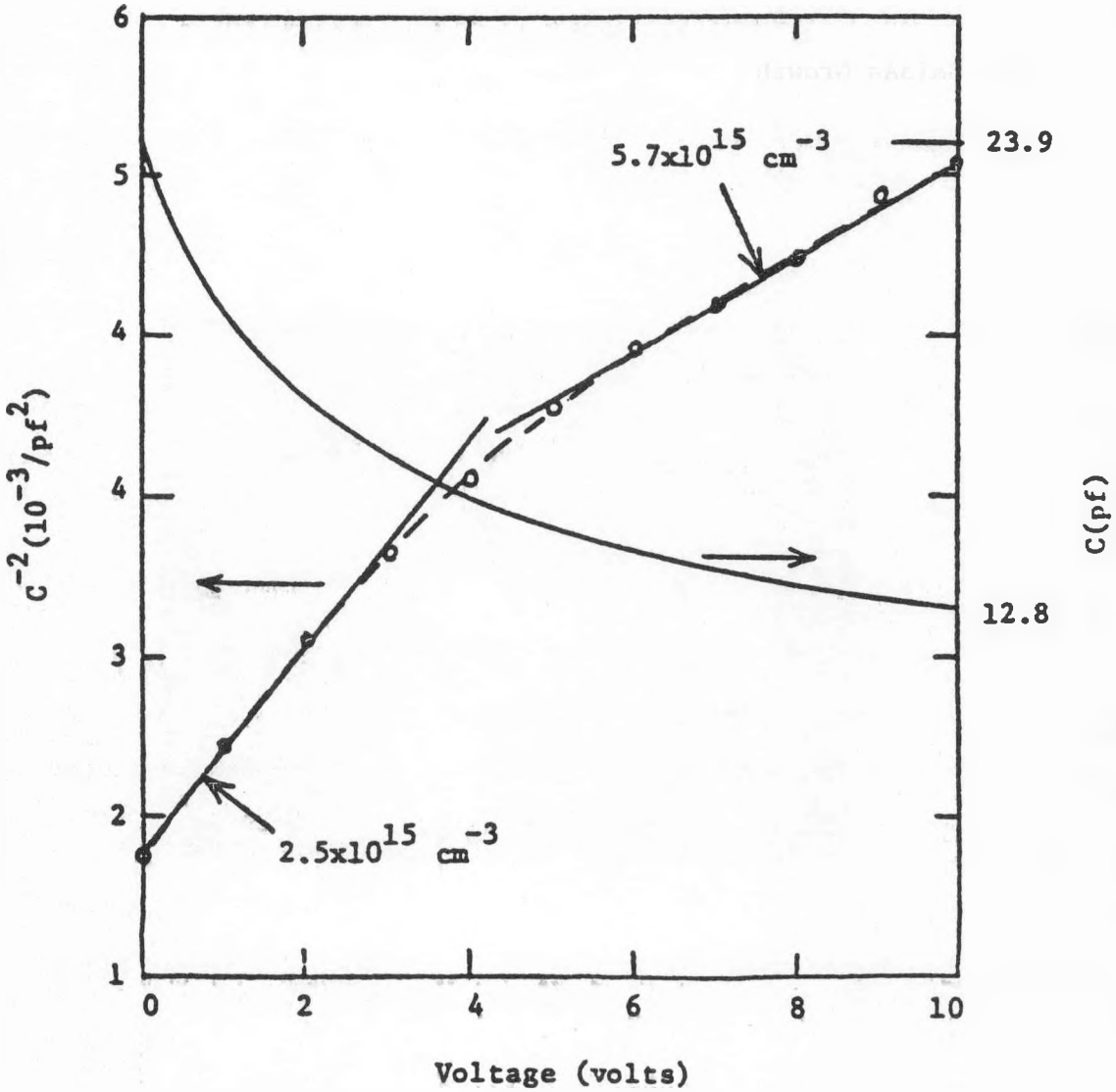

Figure 4.6 C-V Data for AlGaAs Schottky Diode (~20% AlAs)

results with the background doping being n-type and in the range of 1 to 5 × $10^{15}cm^{-3}$.

4.3 GaInAs Growth

As reported previously, difficulties had been encountered in the growth of GaInAs layers with large InAs compositions. These problems now appear to have been overcome with the design of a new reactor tube which has a very short region for the premixing of the Group III and Group V gases before entry into the large reactor tube. Successful growths have now been achieved for pure InAs on GaAs as well as GaInAs with InAs compositions up to 30%. Figure 4.7 shows x-ray diffraction data for pure InAs grown on GaAs. As can be seen, the InAs is of sufficient quality to observe both peaks in the x-ray data. Figure 4.8 shows corresponding data for GaInAs samples with 13% and 28% InAs. In these cases the two peaks are not resolved. This may indicate some variations in the InAs composition of the grown layers. Table 4-1 summarizes data for several GaInAs layers. The surface appearance of many samples has been cloudy as indicated. The surface appearances tend to improve when the optimum growth conditions are obtained.

4.4 GaAsSb Growth

The growth of GaAsSb layers on GaAs has been underway during the last half of the contract period. The work was delayed for several months when the trimethylantimony source was depleted and a new source could not be obtained for several months. The results reported here are thus very preliminary in nature.

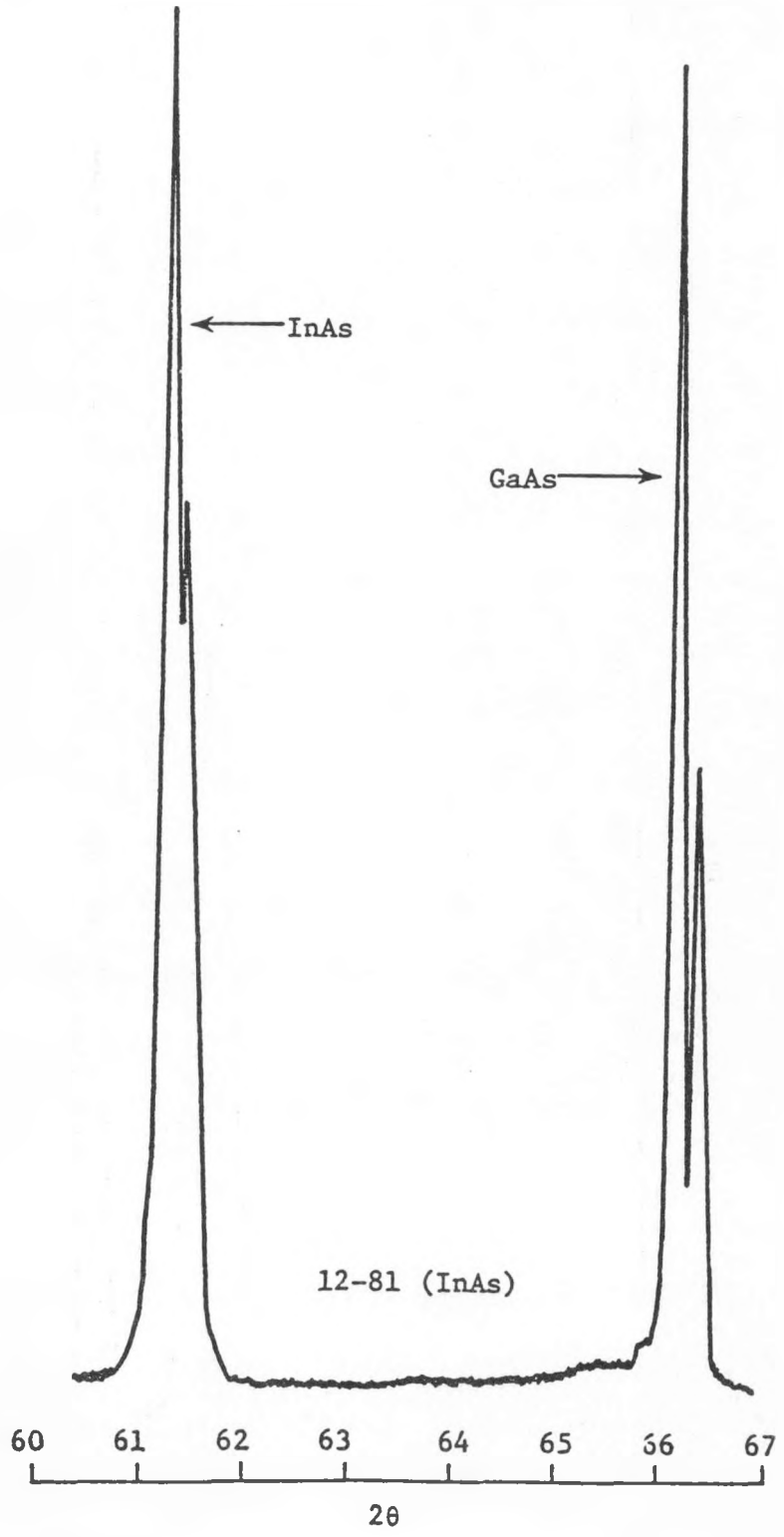

Figure 4.7 X-ray Diffraction Data for InAs on GaAs

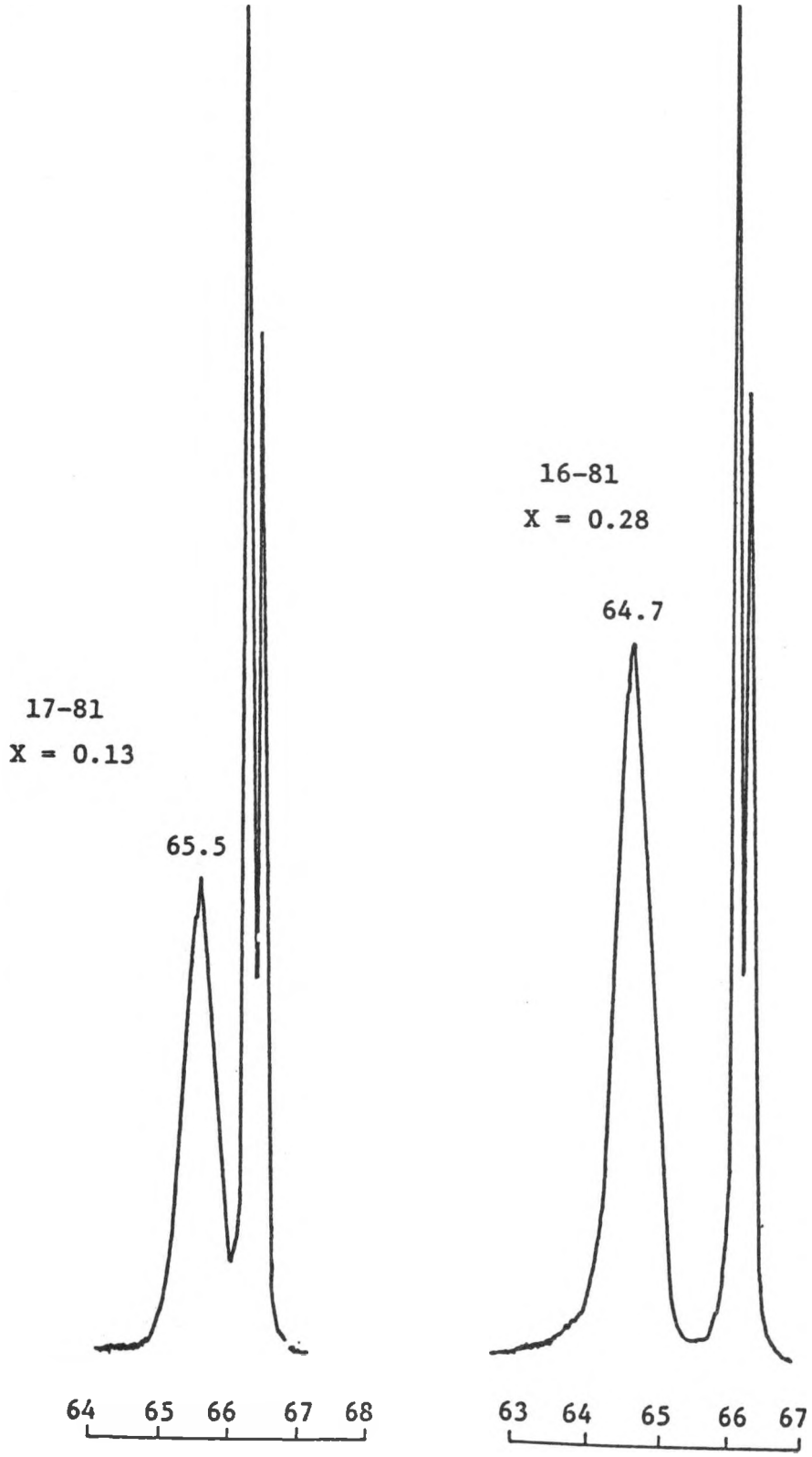

Figure 4.8 X-ray Data for Two $Ga_{1-x}In_xAs$ Layers on GaAs Substrates

Table 4-1. X-RAY DATA ON GaInAs

Sample No.	Angle of Peak (2θ)	% of In*	Surface Appearance
02-80	65.4	14.9	shiny
06-80	65.5	13.0	cloudy
07-80	65.7	9.1	cloudy
13-80	65.8	7.2	shiny
14-80	65.7	9.1	shiny
4-81	65.68	9.5	very shiny
12-81	61.27	100	smooth
13-81	61.27	100	smooth
15-81	64.6	30.5	cloudy
16-81	64.7	28.5	cloudy
17-81	65.5	13.0	cloudy

*Calculated from x-ray data

X-ray diffraction data for a sample with about 5% GaSb in GaAs is shown in Figure 4.9. The peak at 65.9° is very sharp and both K-α peaks are resolved indicating a good structural quality of the layers. Similar data for two layers with compositions of about 72% and 30% GaSb in GaAs are shown in Figure 4.10. The peaks are very broad indicating a poor structural quality of the layers. However, these compositions are much larger than the 10-15% desired in the cascade solar cell structure.

4.5 Summary

Much of the work during the past year was spent on the growth of AlGaAs and GaInAs for potential use in an AlGaAs/GaInAs cascade solar cell. Because of the large lattice mismatch between the two active cells, it was decided during the contract to terminate this work and concentrate on GaAsSb and AlGaAsSb.

The OM-CVD results on GaAsSb are very preliminary in nature. Compositions up to 72% GaSb in GaAsSb have been achieved, but the quality of the layers is not very good. The results, however, are encouraging to the point of expecting that good quality layers with GaSb compositions in the range of 10-15% can be achieved with future work.

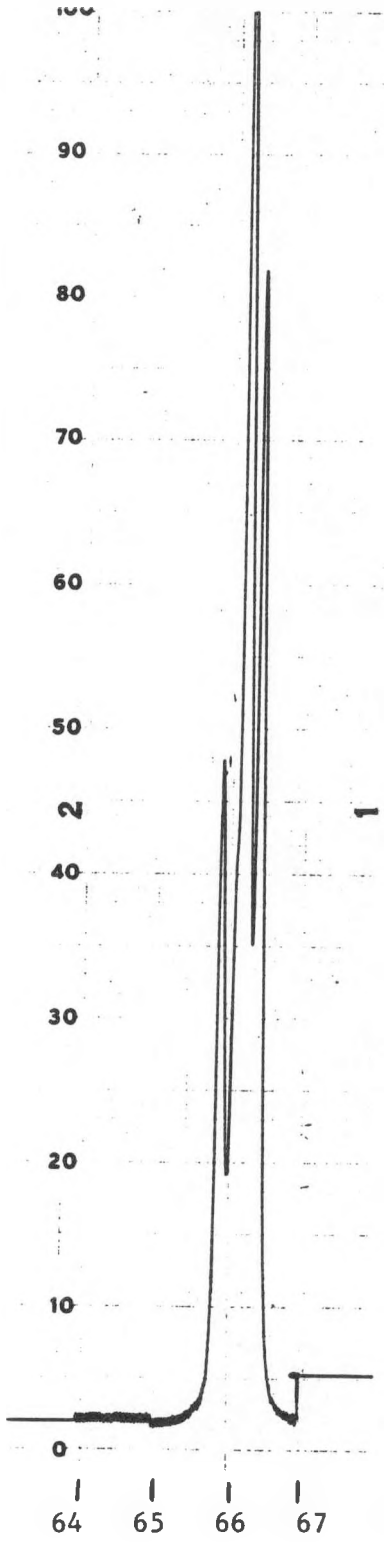

Figure 4.9 X-ray Diffraction Data for Small GaSb Compositions

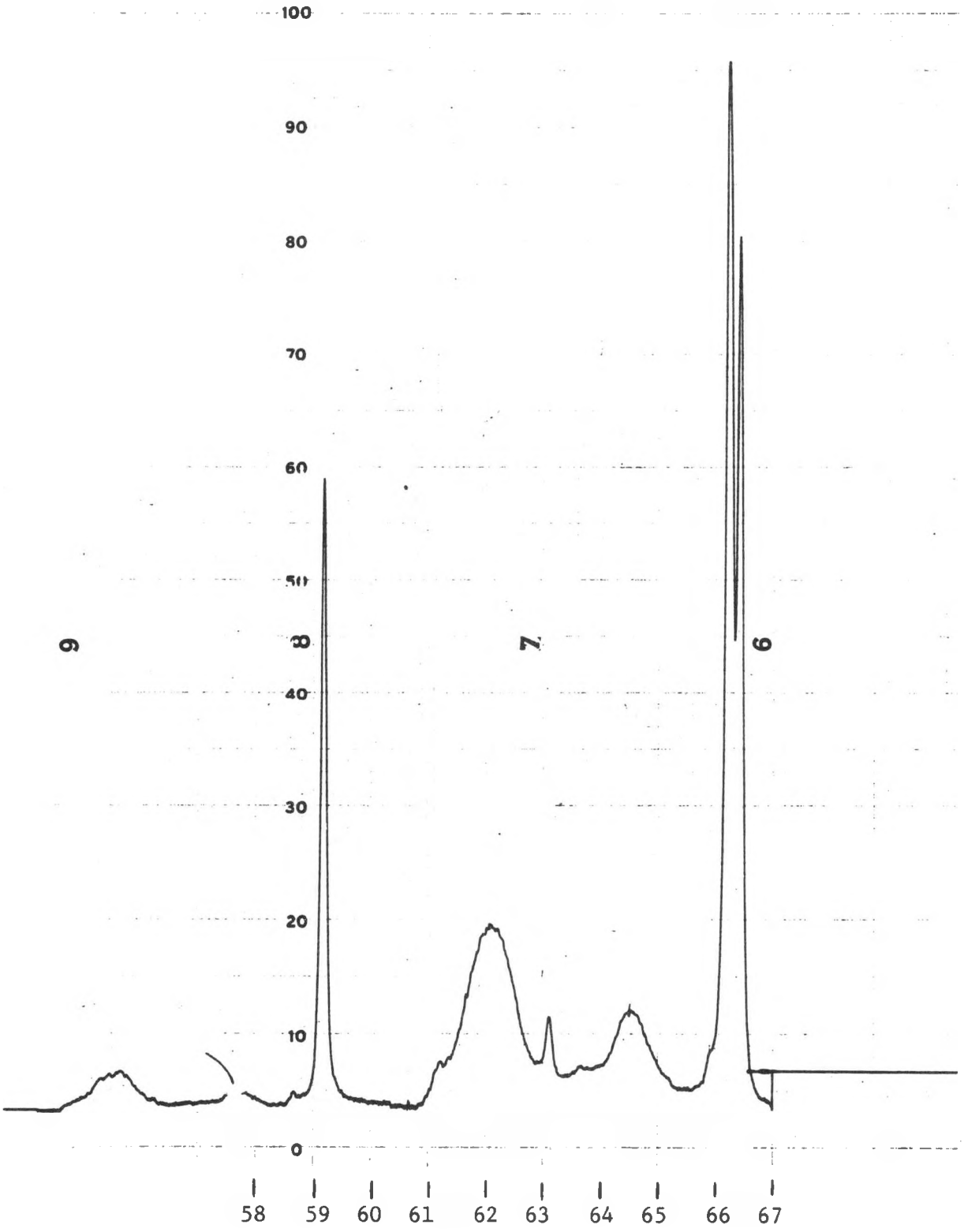

Figure 4.10 X-ray Diffraction Data for Large GaSb Compositions

Blank Page

REFERENCES

1. S. M. Bedair, S. B. Phatak, and J. R. Hauser, IEEE Trans. on Electron Devices, ED-27, 4, Apr. 1980, pp. 822-31.
2. M. F. Lamorte and D. H. Abbott, Solid State Electronics, 22, 1979, pp. 467-73.
3. M. F. Lamorte and D. H. Abbott, IEEE Trans. on Electron Devices, ED-27, 4, Apr. 1980, pp. 831-40.
4. Novel Concentrator Photovoltaic Converter System Development, Final Report for the period Jan. 1978-Jan. 1979, Sandia Contract 07-7149, Research Triangle Institute, Mar. 1979.
5. Novel Concentrator Photovoltaic Converter System Development, Final Report for the period Jan.-Aug. 1979, Sandia Contract 07-7149, Research Triangle Institute, Sept. 1979.
6. Research on High Efficiency Cascade Solar Cells, Annual Report for the period July 1979-June 1980, SERI Contract XM-9-8136-1, Aug. 1980.
7. S. M. Bedair, S. B. Phatak, M. L. Timmons, J. Chiang, and J. R. Hauser, Proc. 14th IEEE Photovoltaic Spec. Conf., 1980, p. 337.
8. S. Fujita, S. M. Bedair, M. A. Littlejohn, and J. R. Hauser, J. Appl. Phys. 51, 1980, p. 5438.
9. R. W. Wagner, J. Appl. Phys. 49, 1978, p. 173.
10. S. M. Bedair, J. Appl. Phys. 50, 1979, p. 7267.
11. S. M. Bedair, J. R. Hauser, M. F. Lamorte, S. Phatak, M. L. Timmons, J. E. Andrews, and M. Simons, Interim Technical Report, prepared for Air Force Aeropropulsion Laboratory, Wright Patterson AFB, OH, Contract No. F-33615-78-C-2077, Oct. 1979, p. 35.

12. G. A. Antypas and R. L. Moon, J. Electrochem. Soc., Vol. 121, No. 3, Mar. 1974, pp. 416-418.

13. Y. Nishitani, K. Abita, A. Yamaguchi, and T. Kotani, J. Electrochem. Soc., Vol. 127, No. 4, Apr. 1980, pp. 949-952.

☆U.S. GOVERNMENT PRINTING OFFICE: 1981-740-145/2464